1991

# Variability in fatigue crack growth and fracture toughness properties in a ceramic reinforced metal-matrix composite

Eda Emine Topur
*Lehigh University*

# VARIABILITY IN FATIGUE CRACK GROWTH AND FRACTURE TOUGHNESS PROPERTIES IN A CERAMIC REINFORCED METAL-MATRIX COMPOSITE

by

Eda Emine Topur

A Thesis

Presented to the Graduate Committee

of Lehigh University

in Candidacy for the Degree of

Master of Science

in

Applied Mechanics

Lehigh University

1990

This thesis is accepted and approved in partial fulfillment of the requirements for the degree of Master of Science in Applied Mechanics.

Dec. 6, 1990
(date)

Prof. Robert P. Wei
(Professor in charge)

Prof. Robert P. Wei
(Chairman of Department)

## ACKNOWLEDGMENT

I would like to express my gratitude to Dr. Robert P. Wei. As my advisor, his guidance and insight for this research project was invaluable. Special thanks must go to Dr. Ming Gao for his many contributions to numerous areas of this work. His assistance with the fracture mechanics experiments, with the fractographic studies, along with his patience, is greatly appreciated. This work could not have been accomplished without him. Acknowledgment must also go to Mr. Carl Miller for providing extensive assistance with the technical experiments. I would also like to thank Mr. Gary Chin for providing me with the results of his work on microstructure.

Support for this research was provided by Dural Aluminum Composites Corporation of ALCAN International. The composites were also provided by ALCAN, and are gratefully acknowledged.

## TABLE OF CONTENTS

## TABLES

## FIGURES

## ABSTRACT

Fatigue crack growth and fracture toughness experiments were carried out on an $Al_2O_3$ particle reinforced aluminum 2014-T6 composite. Fatigue experiments were conducted to examine the variability and influence of environment upon the rate of fatigue crack growth. These tests were carried out in water, water vapor, vacuum, oxygen and air. Experiments were also carried out to study the variability in fracture toughness among the specimens used in the fatigue crack growth experiments and on specimens machined from the fatigue specimens. Companion work was carried out by Gao and Chin for the study of the microstructural behavior of this metal matrix composite as well.

The results indicated variability in the fatigue crack growth rates for specimens tested in the same environments. Scatters among specimens tested in the same environment ranged by factors of 2 to 9. The differences in crack growth rates suggested a possible correlation with variability in fracture toughness. Due to the scatter, environmental effects could not be established. The data in vacuum, however, appeared to be faster than those in the other environments. This unexpected behavior was not understood and needs to be studied further.

Variability was also observed in the fracture toughness data. This variability was found to depend on the location of the specimens (top versus bottom of the cast ingot). The bottom of the cast ingots

displayed higher average fracture toughness, $K_c$ = 21.5 MPa-$m^{1/2}$, and greater variance, $S^2$ = 2.9, than the top of the cast ingots, which had an average toughness value of $K_c$ = 20.3 MPa-$m^{1/2}$ and variance of $S^2$ = 1.1.

These variabilities in fracture toughness data were found to be consistent with the microstructure of the specimens. Optical and SEM micrographs indicated distinct differences in the density and distribution of the alumina particles from the top and bottom of the cast ingots. The top of the cast ingots was observed to have many clustered particles, with non-uniform sizing and spacing, whereas the bottom of the cast ingots was observed to have less dense distributions of alumina particles, that are more uniform in size. The source of the top to bottom variation is believed to result from stratification in the melt ladle. Correlations of this variability observed with fractographic and microstructural observations are being carried out under a separate study to address the role of the microstructural variables.

The variability in fatigue crack growth rates were observed to be governed by the density and distribution of the alumina particles. These variations correlated with the variations observed in fracture toughness.

# I. INTRODUCTION

Aluminum alloys have been used for more than fifty years in automotive, aerospace, sporting goods, and many other structural applications. Corrosion resistance, appearance, lightweight, and fabricability are a few of the properties which make the aluminum economical and attractive [1]. Research has shown, however, that superior properties could be obtained by a combination of aluminum and a dissimilar material. With such a composite, it is possible to acquire superior properties which would result in increases in strength, stiffness and wear resistance [2]. It is no surprise, therefore, that metal matrix composite materials have received increased attention because of these improved properties. The special properties of metal matrix composites have brought on ideas of new products which could change the marketplace [3].

There are three general types of synthetic composites which can be divided into three categories: Dispersion strengthened, particle reinforced, and fiber reinforced [4]. Examples of a particle reinforced metal matrix composite are the $Al_2O_3$ reinforced aluminum alloy and the SiC reinforced aluminum alloy. In these cases, the alloyed aluminum is used as the base material. The volume percentage of the SiC, or of the alumina, particles can range up to about 30 percent, with 10 to 20 percent being typical [3].

A considerable amount of the published research has concentrated on particulate SiC reinforced aluminum alloys. Dural

Aluminum Composites Corporation of ALCAN International, for example, has published research papers on the manufacturing of extruded metal matrix composites using aluminum containing SiC particulates [3,5]. The high cost of these materials precluded their use on a large scale in practice. To reduce cost, a new casting process for producing metal matrix composites, that was simple and inexpensive, was developed [3]. A special pretreatment was used for combining silicon carbide particles with molten aluminum to minimize dissolved gases and oxides [5]. This pretreatment procedure resulted in an extremely uniform distribution of particles in the melt, from which the material was then cast and extruded.

The influence of processing variables on the microstructure of aluminum-silicon carbide particulate composites produced by such a method has been studied [6-9]. It was found, for instance, that cooling rate during solidification affected the distribution of SiC in the final ingot. Lloyd et al. [7] showed that, for 6061-20% SiC solidified at a cooling rate of $20°Cs^{-1}$, the solidification cell size was approximately equal to the SiC particle size. There was little evidence of pushing of the particles by the solidification front. When the cooling rate was slowed to $1.0°Cs^{-1}$, however, solidification cell size several times larger than the SiC particle size was obtained. In this case, there was more particle pushing and clustering of the SiC particles. This non-uniformity in particle distribution produced during solidification is expected to influence the fatigue and fracture properties of metal matrix composites, and needs to be considered.

A number of fatigue studies have been conducted on the SiC particulate reinforced aluminum alloys [10-14]. Davidson [10], for example, investigated fatigue crack growth rates for several aluminum-SiC composites containing 15 and 25 percent of SiC in the matrix. He found that the crack growth rates exhibited a linear, Stage II (Paris) region fitting the function $da/dN = B\Delta K^s$. He found the crack propagated mainly through the aluminum alloy matrix. $\Delta K_{th}$ was observed to be related to yield stress and $SiC_p$ size and volume fraction through the mean free path [10,11]. Further testing, however, needs to be done according to Davidson [10] since not enough data were gathered to substantiate the results.

There has been considerable number of published research on the effects of particulate size, distribution, and volume fraction upon fracture toughness [15-18]. Lewandowski and Liu [15] observed that the micromechanisms of fracture were significantly affected by the details of the matrix microstructure, interface character, and degree of clustering in the material. Increased fracture toughness was observed with increasing particle spacing, provided that the particle size was less than a limiting value, above which unstable crack growth occurred and the toughness lowered [16]. Crack growth fracture toughness was also found to increase with increasing particle size [17].

Because of the ready accessibility and relative low cost of $Al_2O_3$, there has been increased interest in $Al_2O_3$ particulate reinforced aluminum composites for commercial applications [19]. Published literature on $Al_2O_3$ particulate reinforced aluminum

composites, however, is limited.

Klimowicz and Vecchio [20] investigated the influence of aging condition on the fracture toughness and fracture morphology of two metal matrix composites: $Al_2O_3$ reinforced 2014 aluminum alloy and the $Al_2O_3$ reinforced 6061 aluminum alloy. They found that by aging the materials up to the peak aged condition, the yield and tensile strengths increased, while the fracture toughness decreased. Aging the material beyond peak aged condition, the yield and tensile strengths were found to decrease, while the fracture toughness continued to decrease. The 6061 alloy, however, exhibited a smaller change in fracture toughness than the 2014 alloy. The fracture surfaces of the overaged material showed a greater number of shallow microvoids between the fractured alumina particles in this lower toughness condition. They found that the composite material differed significantly from the unreinforced alloy, in the fact that the fracture toughness did not recover or increase when aged beyond peak strength. This was attributed to strain localization caused by the formation of ligaments upon fracture of the alumina particles.

Fatigue in service takes place in many environments. Environment is an important factor influencing the fatigue crack propagation rate in conventional aluminum alloys. Fatigue crack growth rates tend to be reduced, for example, by testing in vacuum or at low temperatures. In corrosive environments, on the other hand, such as water vapor, large increases are observed in fatigue crack growth rates relative to those in an inert environment (for example, vacuum). Fatigue crack growth in an 7075-T6 aluminum alloy is

enhanced by up to an order of magnitude through exposure to aqueous 3.5% sodium chloride compared to dry air [21]. Environmental effects in composite materials, however, are not established. It is therefore important to study the effects of environment on metal matrix composite crack growth behavior.

## II. OBJECTIVES AND SCOPE OF RESEARCH

The initial research program was directed towards the understanding of environmentally assisted fatigue crack growth in the reinforced metal matrix composite. The material used in this study was an $Al_2O_3$ reinforced 2014-T6 aluminum alloy composite extrusion. This research was undertaken to understand the processes and mechanisms of fatigue crack growth response in this composite material. Studies of crack growth behavior, however, led to further considerations of other properties of this material.

Consequently, the objective of this research program was directed towards the study of the variability in fatigue crack growth and fracture toughness properties in this ceramic reinforced metal matrix composite. To achieve these objectives, the research was directed towards (1) the characterization of environmental effect on fatigue crack growth rates, (2) the characterization of variability in fatigue crack growth rates, (3) the characterization of variability in fracture toughness, (4) a correlation between fatigue crack growth behavior and fracture toughness, and (5) a correlation between fracture toughness and the density and distribution of reinforcing particles.

For characterizing the environmental effects on fatigue crack growth rates for the composite material, fatigue tests were performed in the following environments: water, water vapor, air, vacuum, and oxygen. The tests were performed at a frequency of 5 Hz, and load

ratios of R = 0.1, 0.2, and 0.5.

For determining the variability in fracture toughness, fracture tests were performed on compact tension (CT), as well as on wedge opening load (WOL) specimens machined from the (CT) specimens.

For the correlation between fracture toughness and particle density and distribution, microstructural aspects of this metal matrix composite were considered from the preliminary results of a companion work done by Gao [22] and Chin [23].

# III. MATERIAL AND EXPERIMENTAL WORK

## A. Material

An $Al_2O_3$ particulate reinforced 2014-T6 aluminum alloy (metal matrix) composite extrusion was used in this study. The extrusions were furnished by Dural Aluminum Composites Corporation of ALCAN International. Tensile properties, chemical composition, and heat treatment are listed in Table 1.

Typical optical micrographs of polished and unetched surfaces from 2 specimens of this material are shown in Figures 1 to 4. The optical micrographs show the density and distribution of alumina particles as dark phases against the white background of the aluminum matrix. These micrographs were obtained from the companion work by Gao [22].

## B. Specimen

### (i) Fatigue Crack Growth:

For the fatigue crack growth experiments, 40 compact tension (CT) specimens were machined from the extrusions, which were numbered in accordance with Table 2. The first letter in the bar designation (T and B) refers to the position of the extrusion relative to the initial casting: top (T) and bottom (B). The second letter refers to the casting used. The specimens were oriented in the longitudinal (LT) direction. The dimensions of these CT specimens conformed with the ASTM Test Method E647 [24], and are shown in Figure 5. The crack starter notch was introduced into the specimens by means of

electrospark discharge machining (EDM). Prior to receiving the main lot of material, 4 specimens, labeled 2, 3, 4, and 5 were used for preliminary studies. These specimens were of the same material composition and dimensions as those shown in Table 1 and Figure 5. These specimens showed the sensitivity of this composite material towards out-of-plane crack growth. To minimize this problem, the compact tension (CT) specimens were prepared with 1.27 mm deep face-grooves along the expected plane of crack growth.

(ii) Fracture Toughness -- CT and WOL Specimens:

For fracture toughness measurements, the compact tension (CT) specimens designed for fatigue crack growth were used. In addition, to examine the variability in fracture toughness, 2 wedge opening load (WOL) specimens were machined from one of the broken halves of each CT specimen used in the fatigue crack growth experiments (see Figure 6). The dimensions of these WOL specimens conformed with the ASTM standards E-399 [25], and are shown in Figure 7. The crack starter notch was introduced into the specimens by means of electrospark discharge machining.

C. Test Procedure

(i) Fatigue Crack Growth:

The fatigue crack growth experiments were performed at room temperature on an automated closed-loop servo-hydraulic testing machine, operated in load control. The load accuracy was better than $\pm$1%. The fatigue crack growth tests were conducted either under constant amplitude loading, or at a programmed rate of increase in the stress intensity range. In the latter case, the stress intensity

range was controlled using the following equation as suggested by Saxena et al. [26]:

$$K_{max} = K_{maxo} \exp[C(a-a_o)] \quad (1)$$

where $K_{maxo}$ = Initial stress intensity corresponding to $a_o$

$a_o$ = Initial crack length

$a$ = Current crack length

$C$ = Constant with dimensions of 1/length

The control program used for fatigue testing was provided by FTA [27]. The stress intensity factor for the compact tension (CT) specimens were calculated as follows [25]:

$$K_I = \frac{P}{B_{eff}W^{1/2}}F(a/W) \quad (2)$$

$$F(a/W) = (2+a/W)(1-a/W)^{-1.5}\{0.886 + 4.64(a/W) - 13.32(a/W)^2 + 14.74(a/W)^3 - 5.6(a/W)^4\}$$

where $K_I$ = Mode I stress intensity factor

$P$ = Applied load

$a$ = Crack length

$F(a/W)$ = Geometry factor

$B_{eff}$ = Effective specimen thickness

$B_{eff} = (B_oB_1)^{1/2}$

$B_o$ = Specimen thickness

$B_1$ = $B_o$ - face-groove depths

Experiments in vacuum (pressures below 1.3E-5 Pa) were performed in an ultrahigh vacuum (UHV) chamber. Those in oxygen and

water vapor were also performed in the UHV chamber by back-filling it with the respective gases from high-purity sources connected to the chamber. The desired pressures were controlled and monitored with the aid of a capacitance manometer. Tests in air were conducted in the laboratory environment with relative humidity of 40-60 percent. Experiments in water were performed by simply immersing the specimen in distilled water and supplementing the supply by dripping distilled water into the notch from a pipette.

The specimens were precracked in fatigue, in the test environment, to produce a 2.54 mm long crack ahead of the notch tip. This procedure ensured that the crack growth would be free from possible influences of the EDM procedure or the notch geometry. Precracking was performed, at a load ratio of R = 0.1, either under constant amplitude loading at $P_{max} \simeq 6kN$ and f = 8 Hz, or by a programmed increasing K procedure at an initial maximum stress intensity of about 8.8 MPa-$m^{1/2}$ and f = 5 Hz. At the completion of precracking, a stress intensity (K) value of about 11 MPa-$m^{1/2}$ was achieved in each case.

(ii) Fracture Toughness -- CT Specimens:

Fracture toughness measurements were made on some of the CT specimens at the end of the fatigue crack growth experiments. Each of the fatigue tests was terminated prior to specimen fracture, and the specimen was then loaded to failure. Data for load and displacement were recorded and plotted using a program provided by FTA [27].

Some of the specimens tested for fracture toughness exhibited

crack extension before the onset of crack growth instability. This was observed on the load versus displacement charts as a deviation from its original slope. The crack lengths at fracture were estimated from the load-deflection curves using the compliance method described by Hudak and Saxena [28]. The fracture toughness for the CT specimens was calculated from Eq.(2) using the maximum load ($P_{max}$) and the estimated final crack length. Note that since the $K_c$ values were computed using the maximum load of failure and the final crack length, these fracture toughness values represent an upper bound estimate of $K_{Ic}$.

(iii) Fracture Toughness -- WOL Specimens:

Fracture toughness measurements were performed on the WOL specimens using an automated closed-loop servo-hydraulic testing machine. The specimens were precracked in fatigue, in accordance with the ASTM Test Method E399 to extend the crack by about 2.54 mm [25]. Marks were etched onto the specimen surfaces and were used as reference for fatigue precracking. The specimens were then loaded to failure. The program used was provided by FTA [27].

The fracture toughness for the WOL specimens were calculated as follows [25]:

$$K_c = \frac{P_{max}\, a^{1/2}}{BW} F(a/W) \qquad (3)$$

$$F(a/W) = 30.96 - 195.8(a/W) + 730.6(a/W)^2$$
$$-1186.3(a/W)^3 + 754.6(a/W)^4$$

where $K_c$ - Fracture toughness

$P_{max}$ - Maximum load or load at fracture

a - Final crack length

B - Specimen thickness

W - Specimen width

F(a/W) - Geometry factor

The specimens, as for the CT specimens, exhibited crack extension during fracture testing. The crack lengths at fracture were estimated from the load-deflection curves using the compliance method described by Hudak and Saxena [28].

D. Crack Length Measurement

(i) Compact Tension (CT) Specimens:

An AC (alternating current) potential system was used for crack length measurements. This measurement system is based on the fact that the electrical resistance of the specimen increases with increasing crack length [29]. A constant AC current of 1A rms (root mean square) was applied through current leads spot welded to the specimen. Changes in potential were measured by means of potential leads spot welded to the specimen (see Figure 8).

A calibration test was performed by fatigue cracking a specimen in air, while monitoring the potential. A calibration curve was obtained, and the following crack length equation was obtained using the least squares error method:

$$a = C_0 + C_1 V^{*1} + C_2 V^{*2} \qquad (4)$$

where $a$ = Crack length ; in mm.

$C_0$, $C_1$, $C_2$ = Constants for the calibration equation

$V^*$ = Normalized potential

$$V^* = \frac{V - V_0}{V_0}$$

$V$ = Measured potential drop

$V_0$ = Reference potential corresponding to the crack starter notch.

The coefficients were found to be: $C_0 = 12.70$; $C_1 = 37.71$; and $C_2 = 0$. These coefficients were used for the specimens tested in the UHV chamber.

For the experiments in water and in air, another MTS system, without a UHV chamber, was used. Another calibration test had to be performed, since the previous crack length equation can no longer be used, because of differences in the contribution (by the reactive components of the specimen / loading fixture impedance to the A-C potential measurements). These contributions include both the inductive and capacitive coupling [29]. The constants found for the crack length equation (Eqn.4) are as follows: $C_0 = 12.70$; $C_1 = 43.68$; and $C_2 = -24.58$.

(ii) Wedge Opening Load (WOL) Specimens:

For the wedge opening load (WOL) specimens, only precrack measurements were required, since these WOL specimens were used to determine the fracture toughness. Precise measurements were not required for precracking. Hence, scribe marks made on both surfaces of the specimens (2.54 mm away from the notch) were used as reference lines for controlling the extent of precracking.

# IV. RESULTS

## A. Variability in Fatigue Crack Growth Rates

Fatigue crack growth tests were conducted in various environments. The face-grooves, which were used in order to help alleviate the out-of-plane cracking response seen in the preliminary studies done with specimens 2, 3, 4, and 5, was not always successful. Out-of-plane cracking, despite the face-grooves, was encountered. From the 24 specimens tested in various environments, 9 specimens had to be discarded due to out-of-plane cracking. The results are shown in Tables 3, 4, and 5.

From the 15 valid specimens acquired, 4 sets of data were obtained (in vacuum, air, water, and water vapor at 13.3 Pa) to illustrate the variability in fatigue crack growth rate. The results are shown in Figures 9 to 12. The fatigue crack growth rates observed for the specimens in the same environment displayed large variations. This was the case in all four environments. Scatters among specimens tested in the same environment ranged by factors of 2 to 9. The gap between the crack growth rates seemed to widen as higher $K_{max}$ values were reached. Specimens 10 and 48, which were tested in water, were the only two which exhibited similar crack growth rates.

Fatigue crack growth rates were also obtained at a load ratio of R = 0.5 in different environments, as can be seen in Figure 13. The rates for specimens 2 and 11, tested in water vapor and in oxygen

at 66.5 Pa, can be seen in Figure 14.

Because of the variability in crack growth rates, the effect of environment could not be clearly discerned from these results. Nevertheless, the crack growth rates in vacuum appeared to be faster than those in the other environments. This irregularity in rates is not understood. Further works needs to be done upon these findings.

The differences in crack growth rates observed in the same environments and in the $K_{max}$ levels attained suggested a possible correlation with fracture toughness behavior. This possibility was examined and is described in the following section.

### B. Correlation Between Fatigue Crack Growth Behavior and Fracture Toughness

In order to understand the variability observed in crack growth rates, fracture toughness tests were conducted on the compact tension (CT) specimens which were tested for fatigue crack growth experiments.

Out of the 16 valid specimens acquired for fatigue crack growth testing, 7 specimens broke during the fatigue test, and fracture toughness testing was performed on 4 specimens. Fracture toughness measurements were not available on the remaining specimens because those specimens were broken after fatigue testing for crack length measurements. The results are shown in Table 6, and detailed results are given in Appendix I.

The data showed large variability in the fracture toughness values obtained, ranging from 17.6 to 25.6 MPa-$m^{1/2}$. Statistical analysis was used in order to sort out the data. This is considered

in the discussion section. Because of the variability observed, wedge opening load (WOL) specimens were machined from the compact tension (CT) specimens in order to further examine the variability in fracture toughness. This is described in the following section.

It is known that metallurgical factors can have an effect on the fatigue crack propagation rates of materials at high stress intensity factor levels. This occurs because as the stress intensity range ($\Delta K$) increases, the maximum stress intensity factor during each loading cycle approaches the fracture toughness, $K_c$. For the case of tougher materials, for example, they should exhibit lower crack growth rate behavior. This is because tougher materials are usually cleaner, and higher toughness is synonymous with greater crack growth resistance.

This behavior was very apparent with the specimens tested in the four environments. For the specimens tested in water, for example, specimen 13, whose $K_c$ value was measured to be 23.3 MPa-$m^{1/2}$, exhibited significantly lower fatigue crack growth rate than the other two specimens whose values were measured to be 16.7 and 18.1 MPa-$m^{1/2}$.

C. Fracture Toughness Data for WOL Specimens

Fracture toughness tests were conducted on the wedge opening load (WOL) specimens machined from 18 compact tension (CT) specimens. Two of the 36 WOL specimens (specimens 17A and 2A) fractured during precracking. The remaining 34 specimens were tested, and the results are shown in Table 7. Detailed results are given in Appendix II.

The data, as was the case for the CT specimens, showed large

variability, with fracture toughness values ranging from 17.6 to 23.9 MPa-$m^{1/2}$. Statistical analysis was used in order to sort out the data obtained on the WOL specimens, as was done for the CT specimens. This is considered in the discussion section.

# V. DISCUSSION

## A. Variability and Source

Bar graphs were created to show the distribution in fracture toughness values for the compact tension (CT) and the wedge opening load (WOL) specimens. The bar graphs were organized to reflect the location of the specimens relative to the top and bottom of the cast ingots. Statistical analysis of data from each extruded bar was made. The mean and variance of the fracture toughness, and the estimated 95% confidence interval for the mean were obtained for each bar. These values are shown along with fracture toughness data in Figures 15 to 18 for the CT specimens, and Figures 19 to 22 for the WOL specimens.

There appear to be differences in the average value and variance of fracture toughness from the top and bottom of the cast ingots. The $K_c$ values for the bottom of the cast ingots have a higher average than the top of the cast ingots. This is the case for the compact tension (CT) and the wedge opening load (WOL) specimens. The variability also appears to be much higher for specimens from the bottom of the cast ingots than those from the top for both geometric configurations.

Student's t-test was employed on the data from the wedge opening load (WOL) specimens to determine if the observed differences in fracture toughness between the top and bottom of the cast ingots are significant. Note that the test could not be used for the

compact tension (CT) specimens due to insufficient data. Student's t-test was used to first determine if there were differences in average $K_c$ between bars from the top of two cast ingots. The same was done for data from the bottom of two cast ingots. These tests showed the average values to be equal at the 95% confidence interval in each case. Data from the top and bottom of the cast ingots, therefore, were pooled separately and tested for possible differences. The average and variance for specimens from the top of the cast ingots were found to be $K_c$ = 20.3 MPa-$m^{1/2}$ and $S^2$ = 1.1. The average and variance for specimens from the bottom of the cast ingots were found to be $K_c$ = 21.5 MPa-$m^{1/2}$ and $S^2$ = 2.9. The difference between the mean values and variances in fracture toughness for the top and bottom of the cast ingots were found to be statistically significant.

Variability in fracture toughness appeared to depend on the location of the specimens (i.e. top versus bottom of the cast billet). Variability was also observed across the thickness and along the length of the extrusions. There did not appear, however, to be a consistent trend in either case. The source of this variability is most likely related to the density and distribution of the reinforcement alumina particles.

To investigate the effects of the alumina particles, optical micrographs were taken during a companion study by Gao [22]. The specimens were prepared by sectioning them so that each direction would be represented. The micrographs obtained exhibited significant differences in microstructure between the top and bottom of the cast

ingots. The specimens from the top of the cast ingots (specimen 44, for example) were observed to have many clusters of alumina particles. The alumina particles were also observed to have a wide range of sizes. The specimens from the bottom of the cast ingots, however, (such as specimen 24) were observed to have lower density of alumina particles, and the particles were more uniform in size. Increased alumina particle spacing was also observed for these specimens. The optical micrographs for specimens 24 and 44 can be seen in Figures 1 to 4.

SEM microfractographs were also obtained from the compact tension (CT) specimens 24 and 44 tested in water vapor at 13.3 Pa, and were analyzed by Gao [22] and Chin [23]. The micrographs were analyzed at a stress intensity level of $K_{max}$ = 15 MPa-$m^{1/2}$. The results, shown in Figures 23 to 26, indicate the distinct differences between top and bottom of the cast ingots as observed in the optical micrographs.

The observed differences in particle size, spacing, and distribution between top and bottom of the cast ingots seem to be consistent with the variability in fracture toughness. Fracture toughness therefore appears to be governed by the density and distribution of alumina particles.

Possible sources of differences between top and bottom of the cast billets is believed to be related to the stratification in the melt. The top to bottom differences in fracture toughness and variability are consistent with top to bottom variations in particle density and distribution in the melt ladle. Because the alumina

particles are heavier than the aluminum, they tend to settle to the bottom of the ladle. Even with stirring, the material at the top would have a lower density of alumina particles. In the casting process, the material from the top of the ladle is first solidified and forms the bottom of the billet, and the material from the bottom of the ladle becomes the top of the billet. This is consistent with the greater amount of alumina particles observed with the optical micrographs for specimens from the top of the billet. Work is continuing to investigate in detail the morphology of the alumina for different specimens by Chin [23].

### B. Role of Reinforcement Particles

The role of reinforcement particles in determining fracture toughness needs to be clarified. Recent studies on particulate reinforced aluminum metal matrix composites suggest properties such as fracture toughness to be strongly dependant upon the morphology of the reinforcement [13-18]. Kamat et al. [16], for example, have shown that, for a constant volume fraction of alumina, the fracture toughness increased with an increase in particulate size for two matrices. The following authors models will be used in an attempt to quantify this relationship: Hahn and Rosenfield [30] and Krafft [32].

The model developed by Hahn and Rosenfield [30] utilized an approximate failure criterion proposed by Rice and Johnson [31]. They assumed crack extension proceeding when the extent of the heavily deformed region is comparable to the width of the unbroken ligaments separating cracked particles. They showed that the stress

intensity factor could be related in terms of particle diameter and volume fraction, leading to a solution of the form given [30]:

$$K_{Ic} = [2\sigma_Y E(\pi/6)^{1/3}D]^{1/2} f_v^{-1/6} \quad (5)$$

where $\sigma_Y$ = Yield stress

E = Modulus of elasticity

D = Particle diameter

$f_v$ = Reinforcement volume fraction

Using an average alumina particle diameter of 9 $\mu$m and volume fraction of 15%, this model predicts a fracture toughness of 36 MPa-$m^{1/2}$. This value is almost twice that observed by direct measurement. This model utilized a linearly elastic-perfectly plastic material and does not represent true material behavior.

The other model, developed by Krafft [32], assumed fracture to occur when the strain within the small ligament ahead of the crack tip equaled the smooth bar tensile instability strain. Krafft introduced the "process zone size" as a material parameter which might be identified with the particle spacing. In this case, the correlation between plane strain fracture toughness $K_{Ic}$ and the process zone size is given by [32]:

$$K_{Ic} = En(2\pi d_T)^{1/2} \quad (6)$$

where E = Modulus of elasticity

n = Strain hardening coefficient

$d_T$ = Process zone size

For estimated strain hardening coefficients of 0.1 to 0.2 [33] and fracture toughness between 17 and 26 MPa-$m^{1/2}$, the model suggests a maximum process zone size of 1 $\mu$m. This is too small in terms of the spacing between individual particles and the particle size (9$\mu$m). The lack of agreement may have resulted from the assumed ductile mode of failure.

To account for brittle behavior, a "brittle" variant is introduced to the Krafft model by replacing the strain hardening exponent with the fracture strain $\epsilon_f$. For a fracture strain of 1 to 2% (see Table 1), and fracture toughness between 17 and 26 MPa-$m^{1/2}$, the model predicts process zone size between 12 to 112 $\mu$m. These values are more consistent with the average spacing between small clusters of alumina particles, rather than between individual particles. This can be observed, for example, as indicated by the marked regions in Figure 27.

The microstructural sensitivity is reflected in variability in fatigue crack growth rates within a given specimen. Fatigue crack growth rates seem to be governed by particle density and distribution. This variation is shown in Figure 28 in relation to the variations in fracture toughness values observed due to specimen location (top versus bottom of cast ingot). Because of variability, it was difficult to study the effect of environment on fatigue crack growth. Additional work needs to be performed to clarify these findings.

# VI. CONCLUSION

The research project was undertaken to study the variability in fatigue crack growth and fracture toughness properties of $Al_2O_3$ particulate reinforced aluminum composites.

Fatigue crack growth rates were obtained in the following environments: air (relative humidity of 40-60 percent), vacuum (pressures below 1.3E-5 Pa), water, water vapor (13.3 Pa), and oxygen. Large differences (up to factors of 9) were observed in the fatigue crack growth rates of specimens tested in the same environments. The difference in crack growth rates seemed to widen as higher stress intensity values were reached for all four environments. These differences suggested a possible correlation with variability in fracture toughness.

Fracture toughness experiments were performed on the specimens used in the fatigue crack growth experiments and on specimens machined from the fatigue specimens. Large variability in the fracture toughness was observed. The average value of fracture toughness and variability were found to depend on the location of the specimens (top versus bottom of the cast billet); being 20.3 MPa-$m^{1/2}$ with $S^2$ = 1.1 for the top and 21.5 MPa-$m^{1/2}$ with $S^2$ = 2.9 for the bottom of the cast billets, respectively. The top to bottom differences in fracture toughness and variability was consistent with top to bottom variations in particle density and distribution that resulted from stratification in the melt ladle. The results are

consistent with the observed differences in density and distribution of $Al_2O_3$ particles between the tops and bottoms of the billets.

There were also considerable variations in fracture toughness through the specimen thickness and along the length of the extrusions. No meaningful correlation between this variability and surface morphology has been established in this case. Correlations of this variability observed with fractographic and microstructural observations are being carried out under a separate study to address the role of the microstructural variables.

Fatigue crack growth rates were also observed to be governed by particle density and distribution. The variability in the rates correlated with variations in fracture toughness. Because of the variability in crack growth rates, environmental effects could not be clearly discerned from the experimental results. Nevertheless, the crack growth rates in vacuum appeared to be faster than those in the other environments. This unexpected behavior is not understood and needs to be studied further.

## Table 1

## Tensile Properties, Chemical Composition, and Heat Treatment of $Al_2O_3$ Reinforced 2014-T6 Aluminum Alloy.

### Tensile Propreties

| Yield Strength (MPa) | Tensile Strength (MPa) | Young's Modulus (GPa) | Elongation (pct) |
|---|---|---|---|
| 484 | 512 | 98 | 2.0 |

### Chemical Composition, Weight Percent

| Alloy | Si | Cu | Mn | Mg | Al |
|---|---|---|---|---|---|
| 2014 | 0.8 | 4.4 | 0.8 | 0.5 | 93.5 |

### Heat Treatment

Solution Heat Treated at 500°C for 1.5 hours.

Quenched in cold water within 15 seconds to room temperature.

Aged at 160°C for 16 hours and cooled in air.

## Table 3

## The Tests Performed in Various Environments

## on the Compact Tension (CT) Specimens

## at a Load Ratio of R = 0.1.

| ENVIRON. | Pressure (Pa) | | | | | | | |
|---|---|---|---|---|---|---|---|---|
| | | 1.3 | 4.0 | 13.3 | 66.5 | 665 | AIR | WATER |
| VACUUM | *- 44<br>*- 23<br>o- 18<br>o- 4 | | | | | | | |
| OXYGEN @ 665 Pa | *- 11<br>o- 21<br>o- 43 | | | | | | | |
| WATER VAPOR | | | o- 53 | *- 24<br>*- 42 | *- 2<br>o- 15 | | *- 54<br>*- 47 | *- 13<br>*- 48<br>*- 10 |

R = 0.1

*- VALID TEST
o- INVALID TEST

## Table 4

## The Tests Performed in Various Environments

## on the Compact Tension (CT) Specimens

## at a Load Ratio of R = 0.5.

| ENVIRON. | Pressure (Pa) | | | | | | | |
|---|---|---|---|---|---|---|---|---|
| | | 1.3 | 4.0 | 13.3 | 66.5 | 665 | AIR | WATER |
| VACUUM | *- 22 | | | | | | | |
| OXYGEN @ 665 Pa | *- 17 | | | | | | | |
| WATER VAPOR | | *- 19 | | *- 20 | | o- 14 | | |

R = 0.5

*- VALID TEST
o- INVALID TEST

Table 5

The Tests Performed in Various Environments

on the Compact Tension (CT) Specimens

at a Load Ratio of R = 0.2.

| ENVIRON. | Pressure (Pa) | | | | | | | |
|---|---|---|---|---|---|---|---|---|
| | | 1.3 | 4.0 | 13.3 | 66.5 | 665 | AIR | WATER |
| VACUUM | | | | | | | | |
| OXYGEN @ 665 Pa | | | | | | | | |
| WATER VAPOR | | | | | o- 3<br>o- 5 | | | |

R = 0.2

*- VALID TEST
o- INVALID TEST

## Table 6

## Fracture Toughness Results from the Compact Tension (CT) Specimens.

| SPECIMEN | $K_c$ (MPa-$m^{1/2}$) | REMARKS |
|---|---|---|
| 02 | 21.9 | BROKE DURING FATIGUE TEST |
| 03 | ---- | OUT-OF-PLANE |
| 04 | ---- | OUT-OF-PLANE |
| 05 | ---- | OUT-OF-PLANE |
| 10 | 18.2 | -- |
| 11 | 19.5 | BROKE DURING FATIGUE TEST |
| 13 | 23.6 | -- |
| 14 | ---- | OUT-OF-PLANE |
| 15 | ---- | OUT-OF-PLANE |
| 17 | 20.4 | BROKE DURING FATIGUE TEST |
| 18 | ---- | OUT-OF-PLANE |
| 19 | 25.0 | BROKE DURING FATIGUE TEST |
| 20 | >20.6 | NO FRACTURE TEST DONE |
| 21 | ---- | OUT-OF-PLANE |
| 22 | >21.8 | NO FRACTURE TEST DONE |
| 23 | >22.0 | NO FRACTURE TEST DONE |
| 24 | >17.3 | NO FRACTURE TEST DONE |

| SPECIMEN | $K_c$ (MPa-$m^{1/2}$) | REMARKS |
|---|---|---|
| 42 | 18.9 | BROKE DURING FATIGUE TEST |
| 43 | ---- | OUT-OF-PLANE |
| 44 | 18.5 | BROKE DURING FATIGUE TEST |
| 47 | 17.6 | -- |
| 48 | 18.4 | -- |
| 53 | ---- | OUT-OF-PLANE |
| 54 | 25.6 | BROKE DURING FATIGUE TEST |

## Table 7

## Fracture Toughness Results from the Wedge Opening Load (WOL) Specimens.

| SPECIMEN | $K_c$ (MPa-$m^{1/2}$) | Remarks |
|---|---|---|
| 02-A | 17.6 | BROKE WHILE PRECRACKING |
| 02-B | 19.1 | -- |
| 10-A | 21.1 | -- |
| 10-B | 19.7 | -- |
| 11-A | 20.1 | -- |
| 11-B | 19.8 | -- |
| 13-A | 20.9 | -- |
| 13-B | 21.2 | -- |
| 17-A | 18.4 | BROKE WHILE PRECRACKING |
| 17-B | 22.6 | -- |
| 18-A | 22.2 | -- |
| 18-B | 20.4 | -- |
| 19-A | 22.7 | -- |
| 19-B | 19.8 | -- |
| 20-A | 21.7 | -- |
| 20-B | 23.8 | -- |
| 22-A | 18.6 | -- |
| 22-B | 21.6 | -- |
| 23-A | 22.9 | -- |
| 23-B | 22.0 | -- |
| 24-A | 21.6 | -- |
| 24-B | 22.6 | -- |

| SPECIMEN | $K_c$ (MPa-$m^{1/2}$) | REMARKS |
|---|---|---|
| 42-A | 21.7 | -- |
| 42-B | 18.1 | -- |
| 44-A | 19.8 | -- |
| 44-B | 19.2 | -- |
| 47-A | 21.9 | -- |
| 47-B | 20.5 | -- |
| 48-A | 19.5 | -- |
| 48-B | 20.2 | -- |
| 53-A | 20.3 | -- |
| 53-B | 23.9 | -- |
| 54-A | 18.9 | -- |
| 54-B | 22.8 | -- |


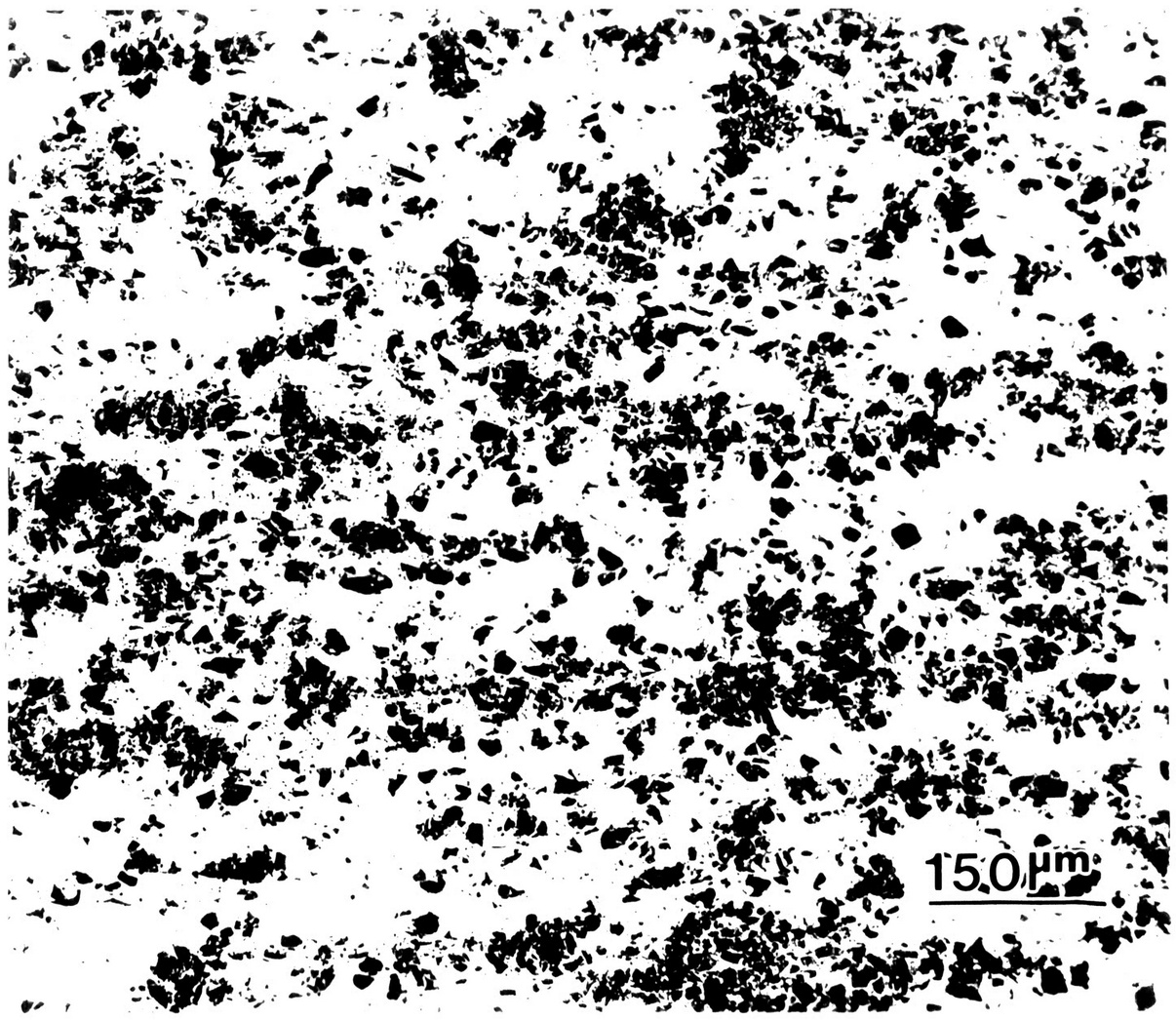


Figure 1: Optical micrographs taken from compact tension (CT) specimen 44. Magnification: 100X


Figure 2: Optical micrograph taken from compact tension (CT) specimen 44. Magnification: 500X

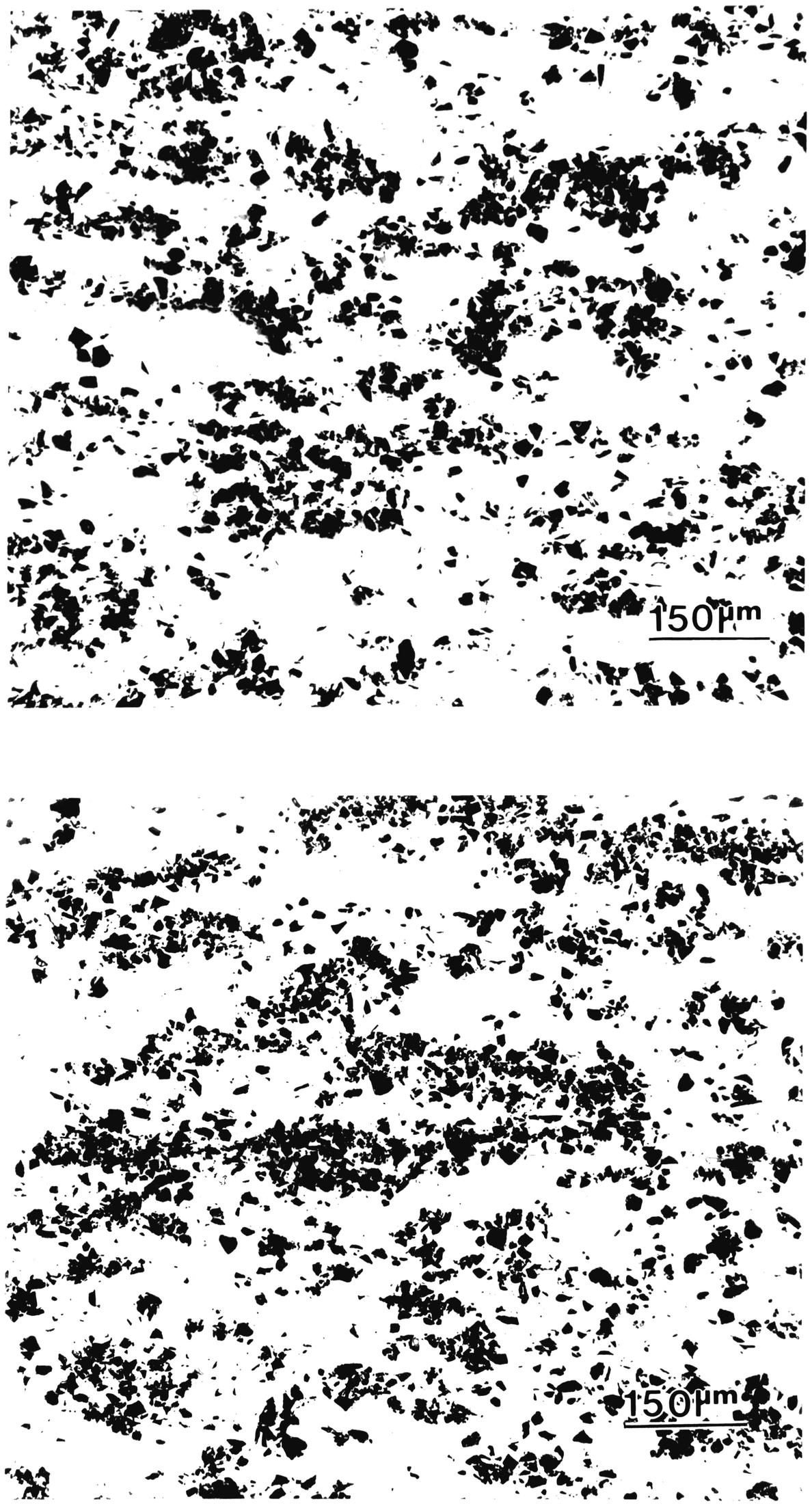


Figure 3: Optical micrographs taken from compact tension (CT) specimen 24. Magnification: 100X

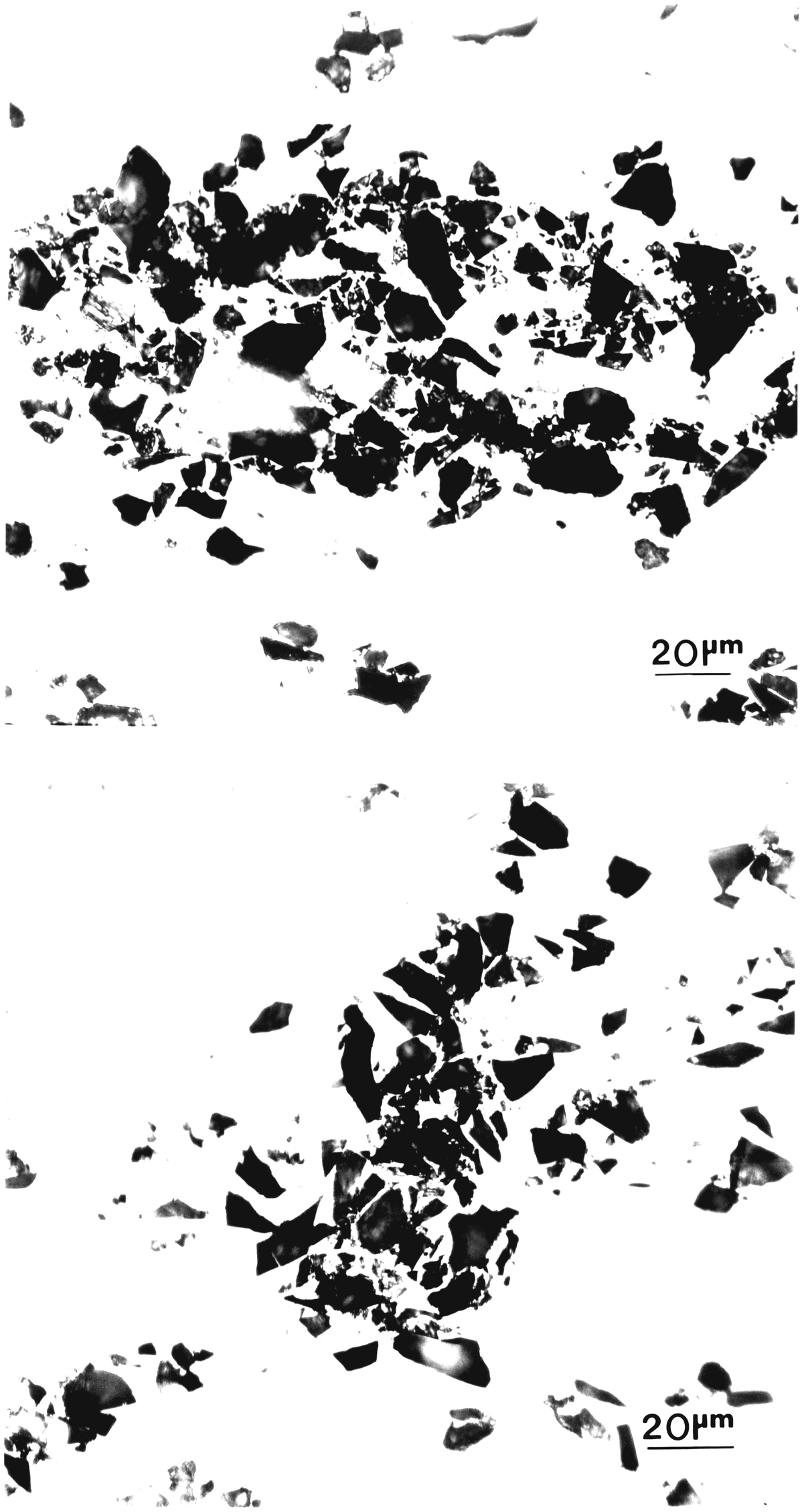


Figure 4: Optical micrograph taken from compact tension (CT) specimen 24. Magnification: 500X

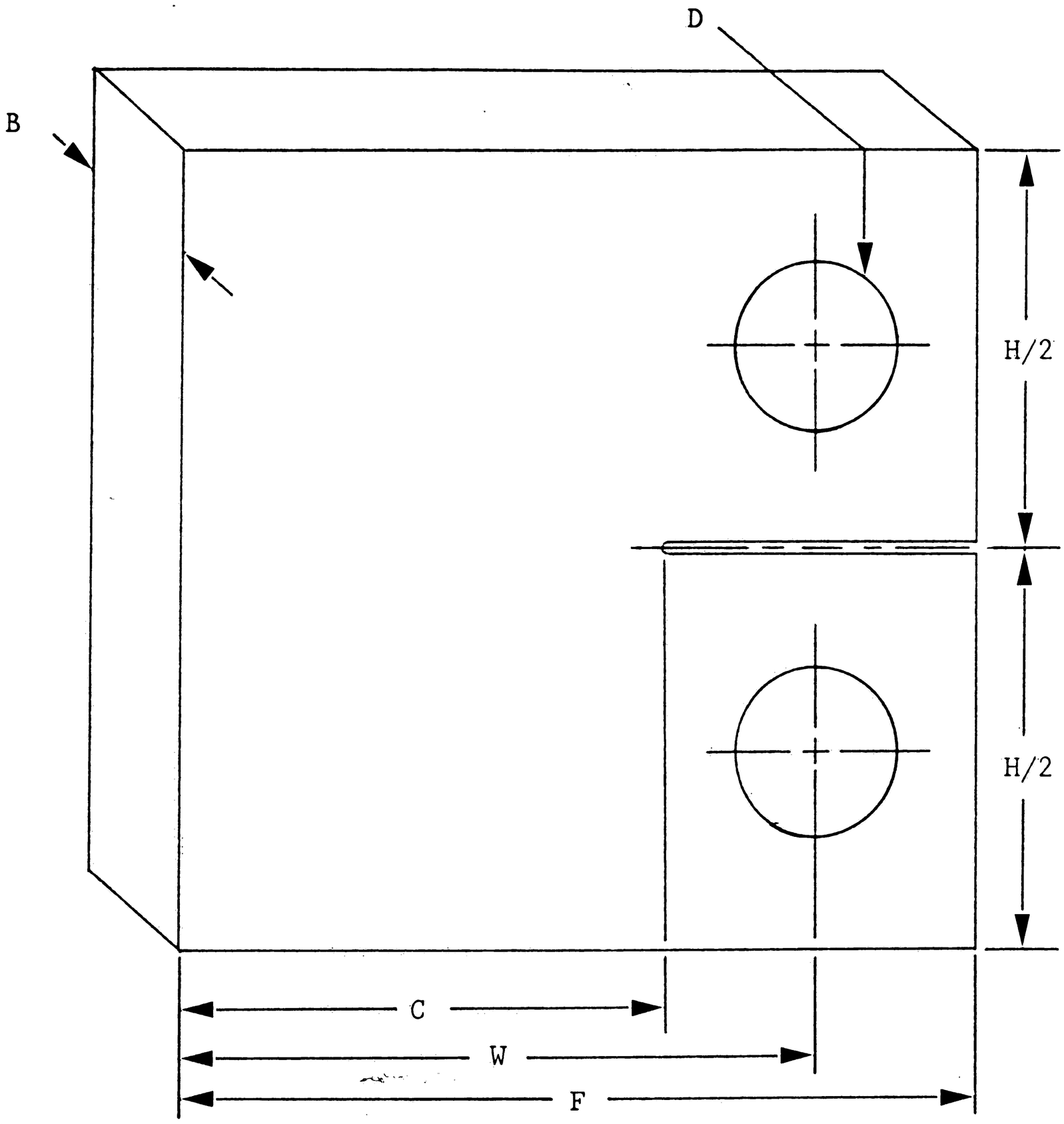


W = 50.8 mm

B = 12.7 mm

H/2 = 30.48 mm

C = 38.1 mm

F = 63.5 mm

D = 12.7 mm

Pre-notched, with root radius of 0.25 mm maximum.

Figure 5: Compact tension (CT) specimens for fatigue testing.

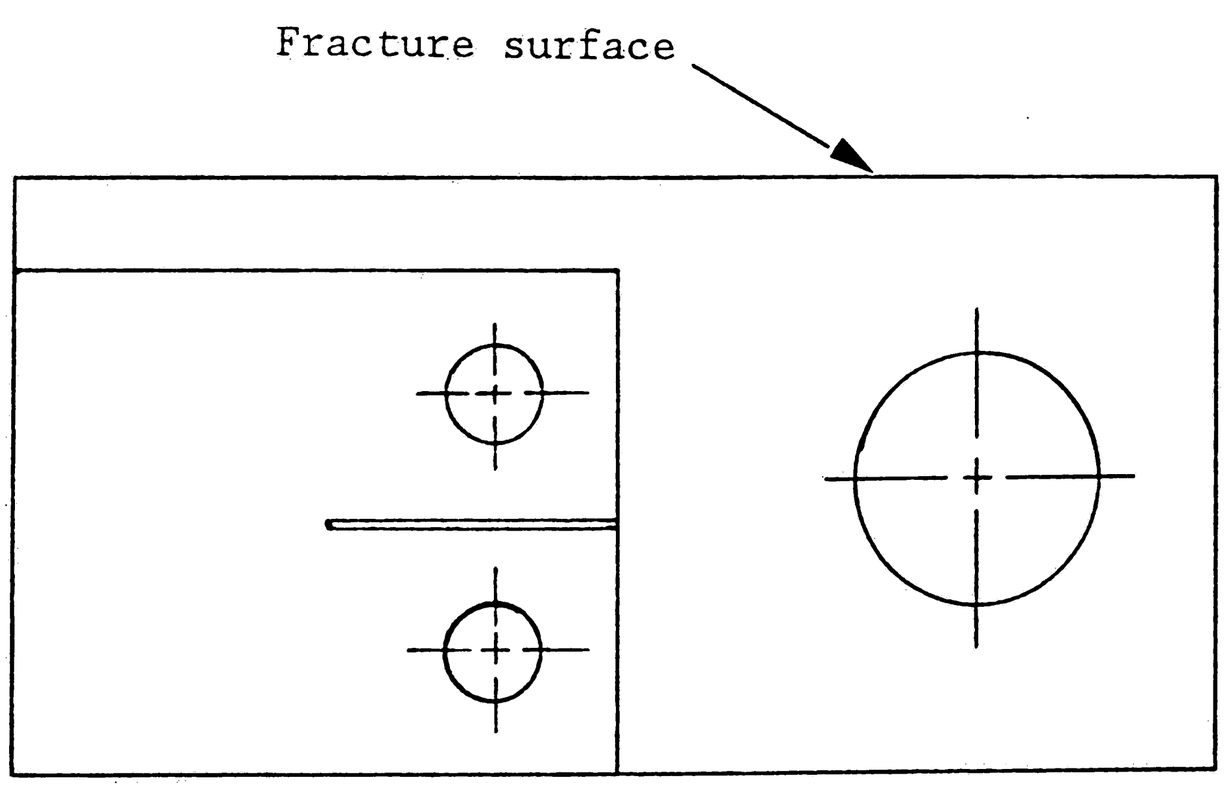


Figure 6: Location of the wedge opening load (WOL) specimens machined from the broken compact tension (CT) specimens.

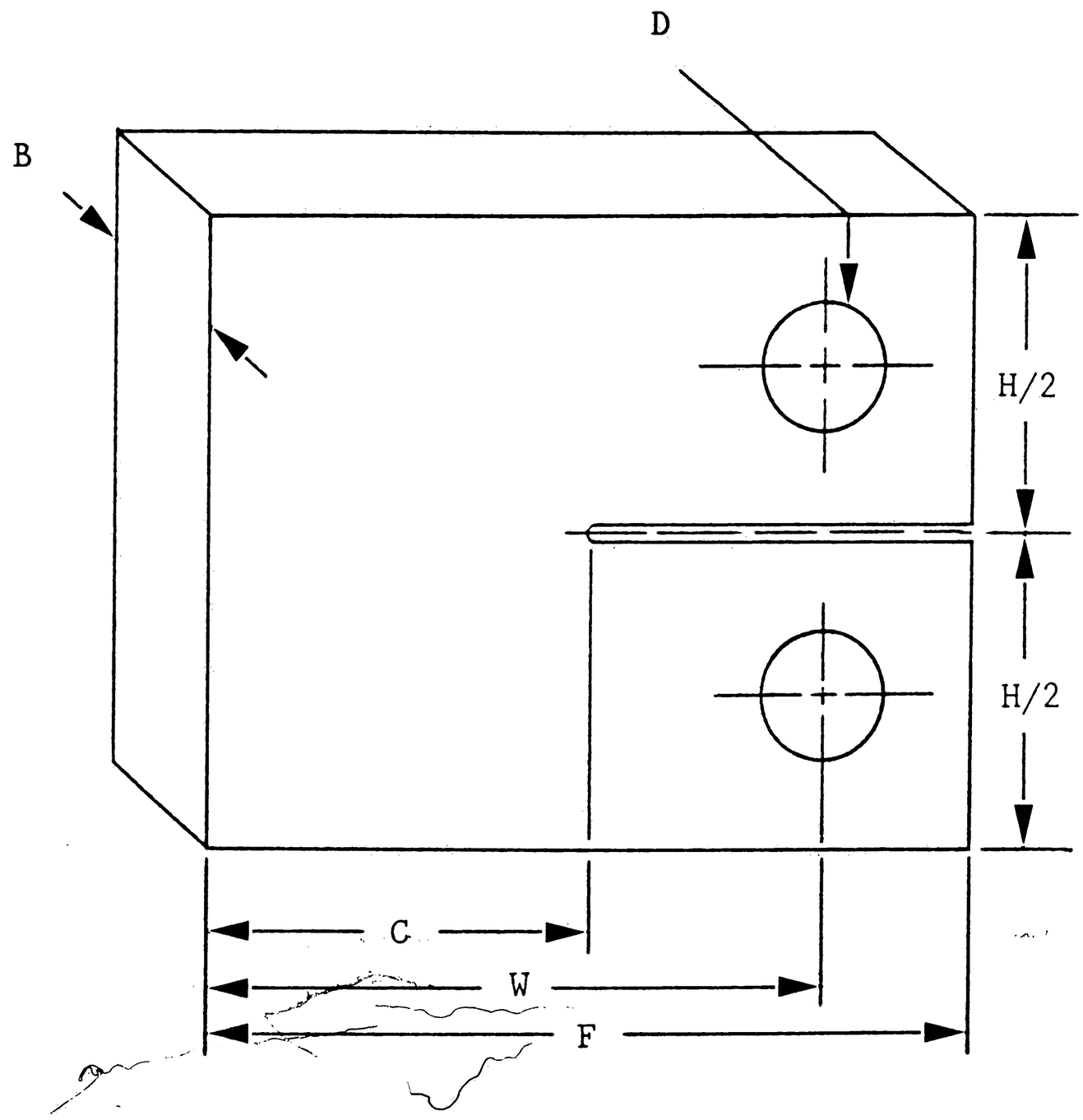


W = 25.4 mm C = 15.24 mm

B = 5.97 mm F = 31.75 mm

H/2 = 12.45 mm D = 4.78 mm

Pre-notched, with root radius of 0.25 mm maximum.

Figure 7: Wedge opening load (WOL) specimens for fracture toughness testing.

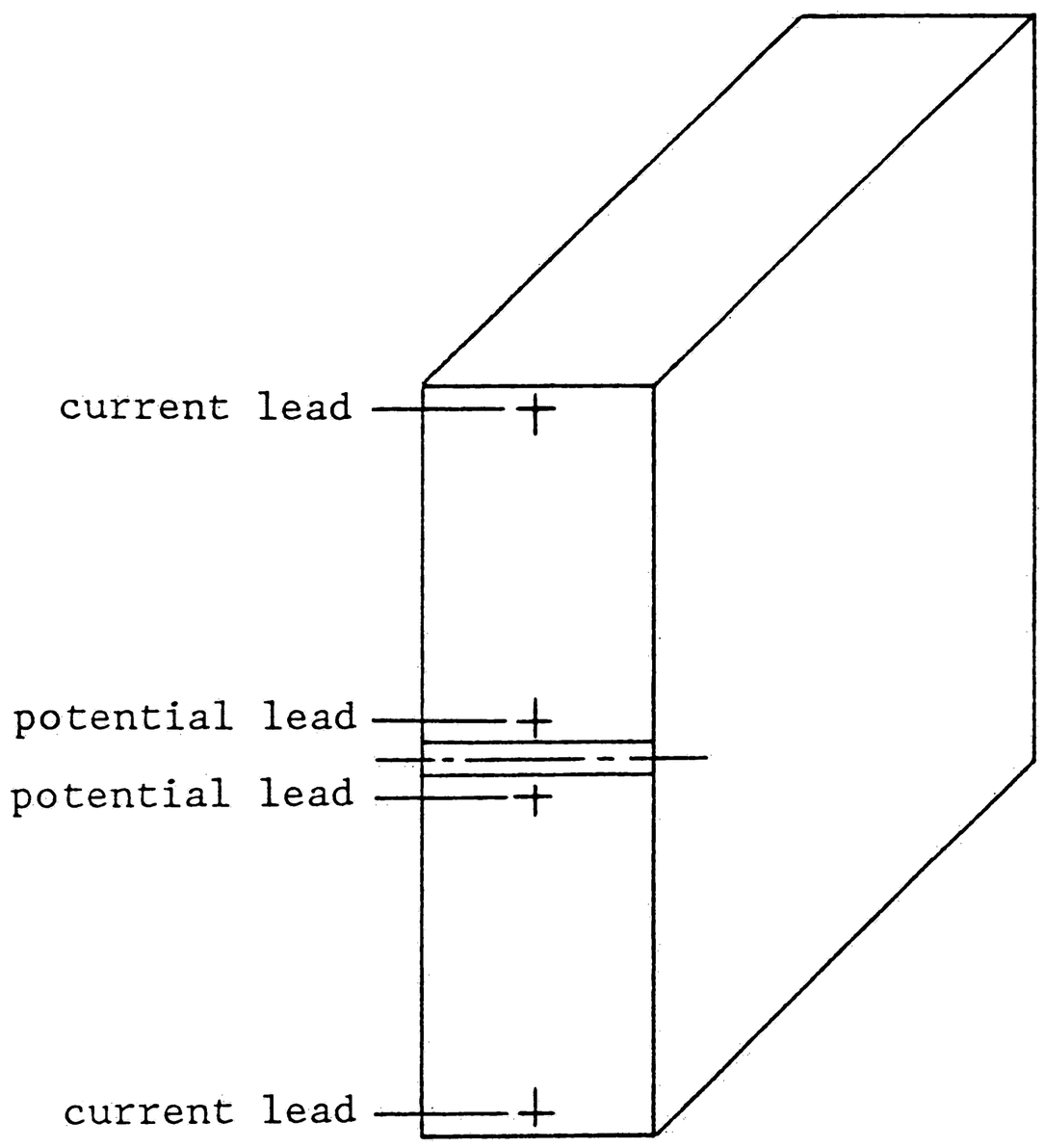


Figure 8: Location of the potential and current leads on the compact tension (CT) specimens.

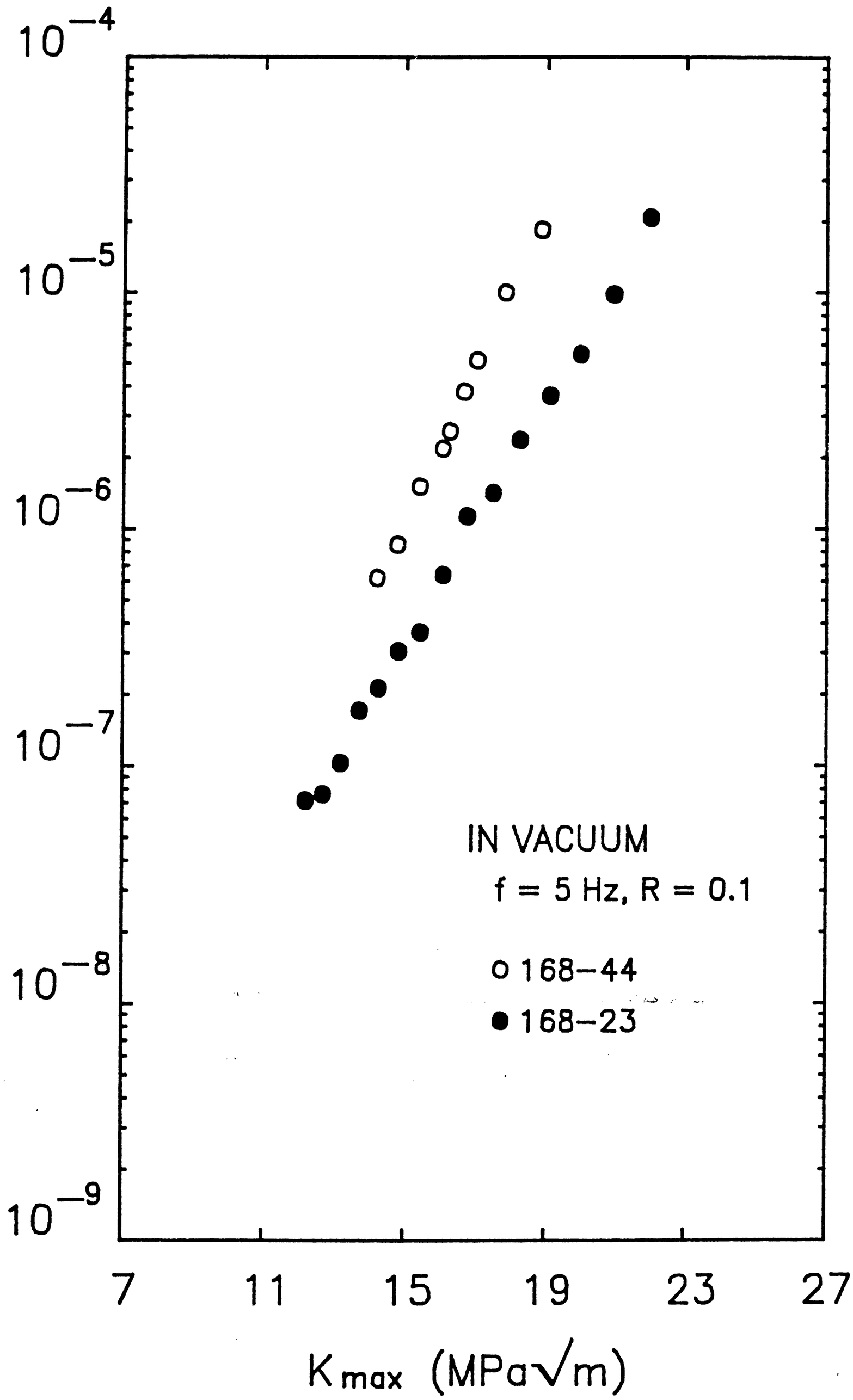


Figure 9: Comparison of fatigue crack growth rate versus $K_{max}$ data for specimens 44 and 23 tested in vacuum at room temperature.

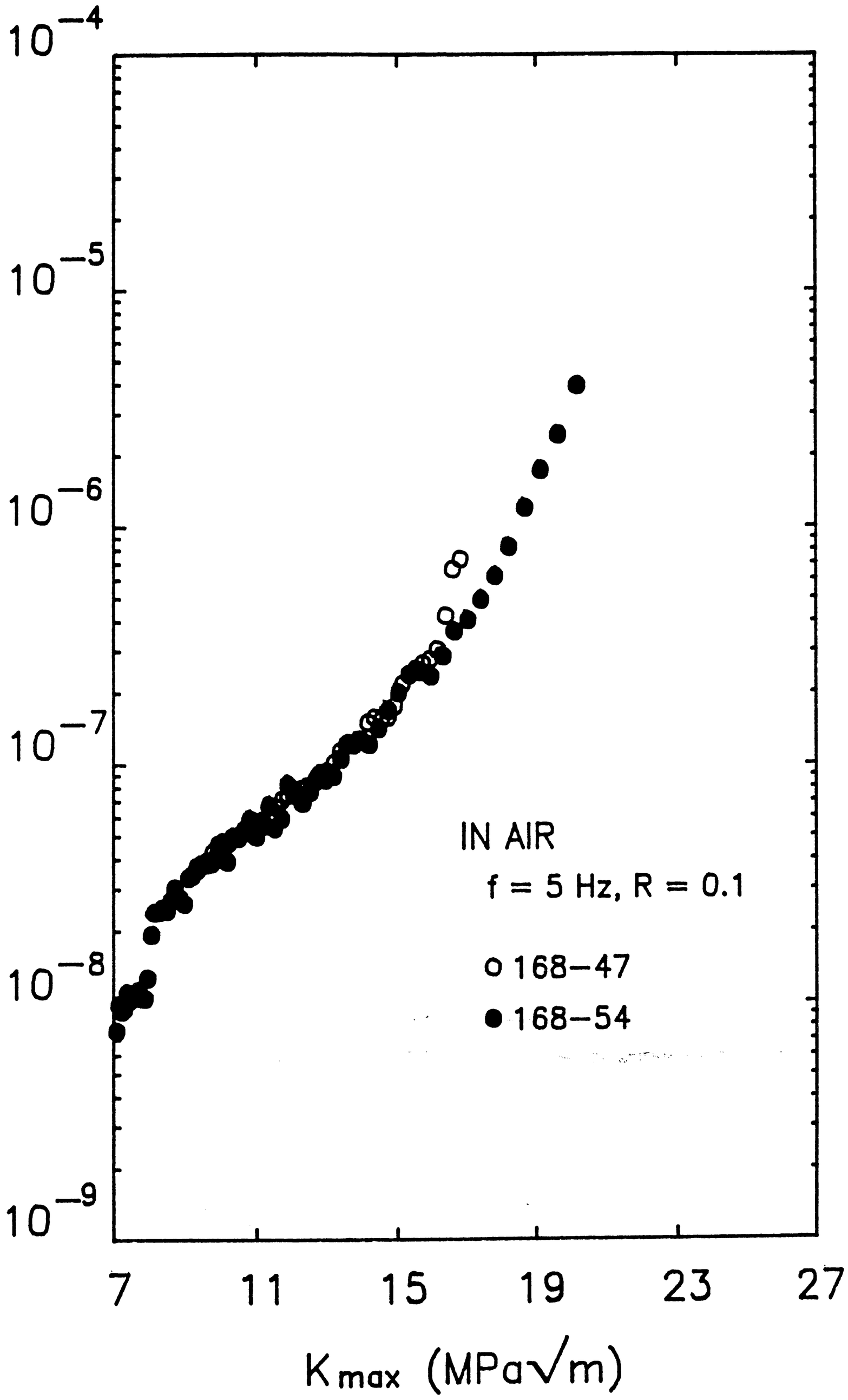


Figure 10: Comparison of fatigue crack growth rate versus $K_{max}$ data for specimens 47 and 54 tested in air at room temperature.

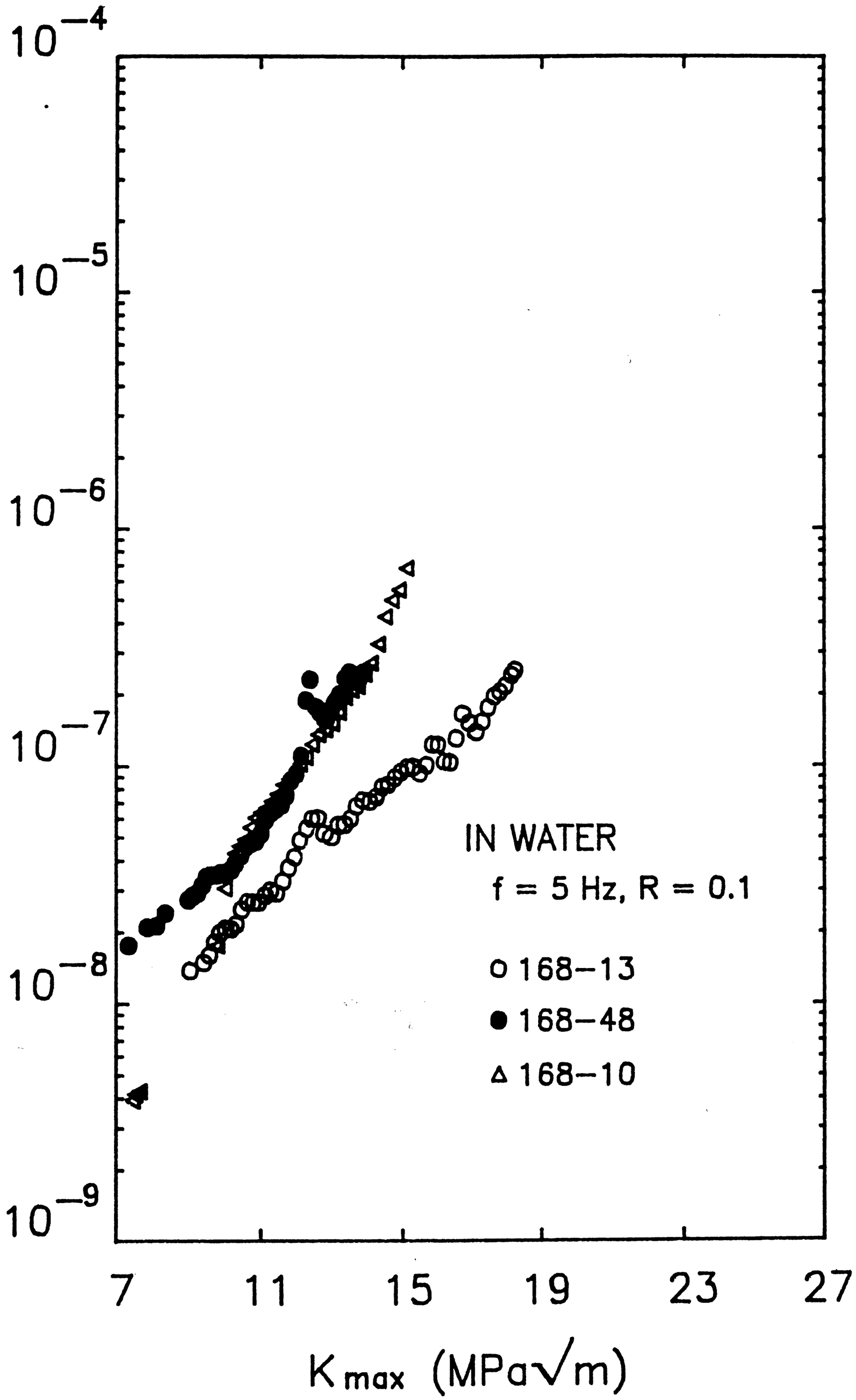


Figure 11: Comparison of fatigue crack growth rate versus $K_{max}$ data for specimens 13, 10, and 48 tested in water at room temperature.

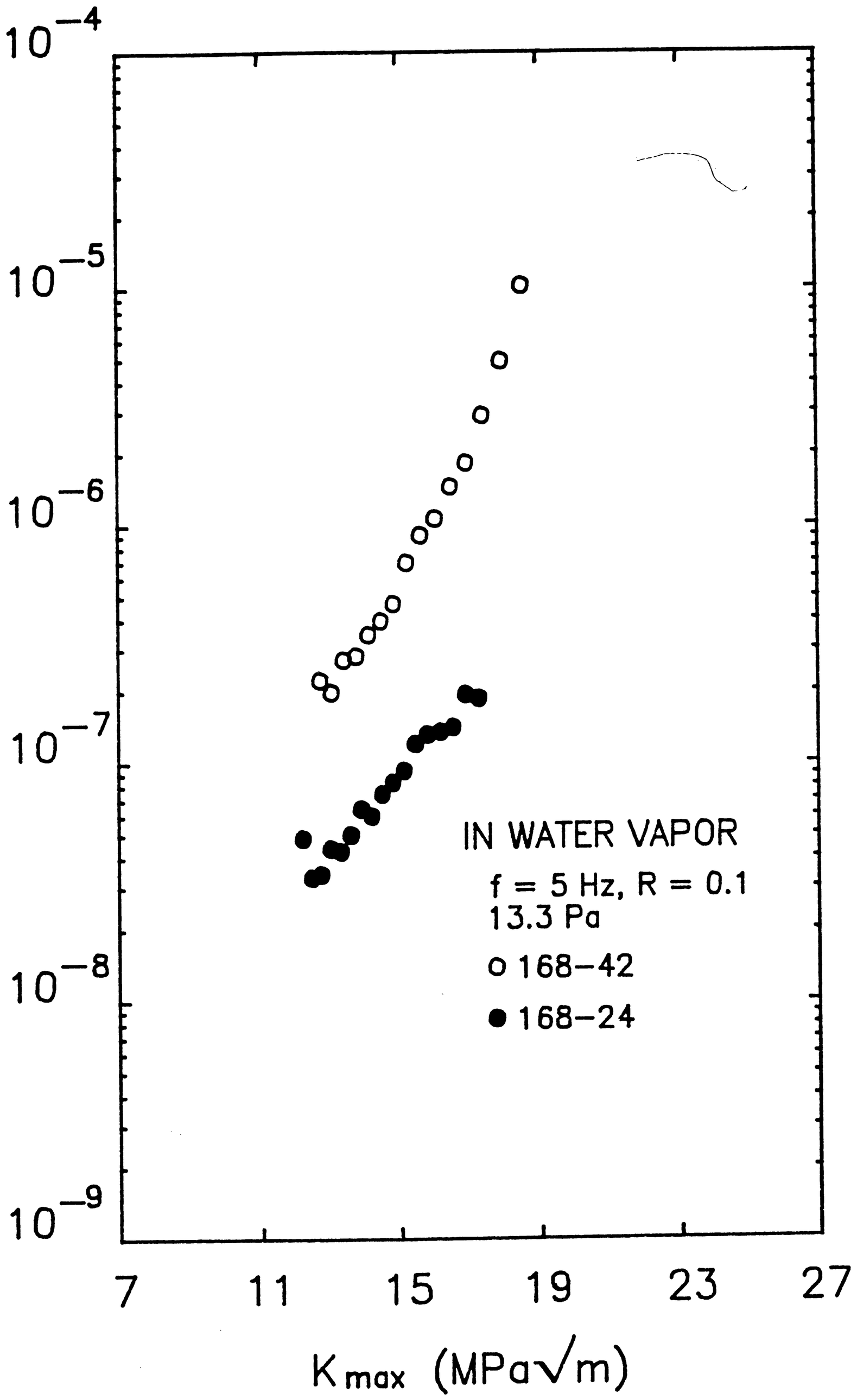


Figure 12: Comparison of fatigue crack growth rate versus $K_{max}$ data for specimens 42 and 24 tested in water vapor at 13.3 Pa.

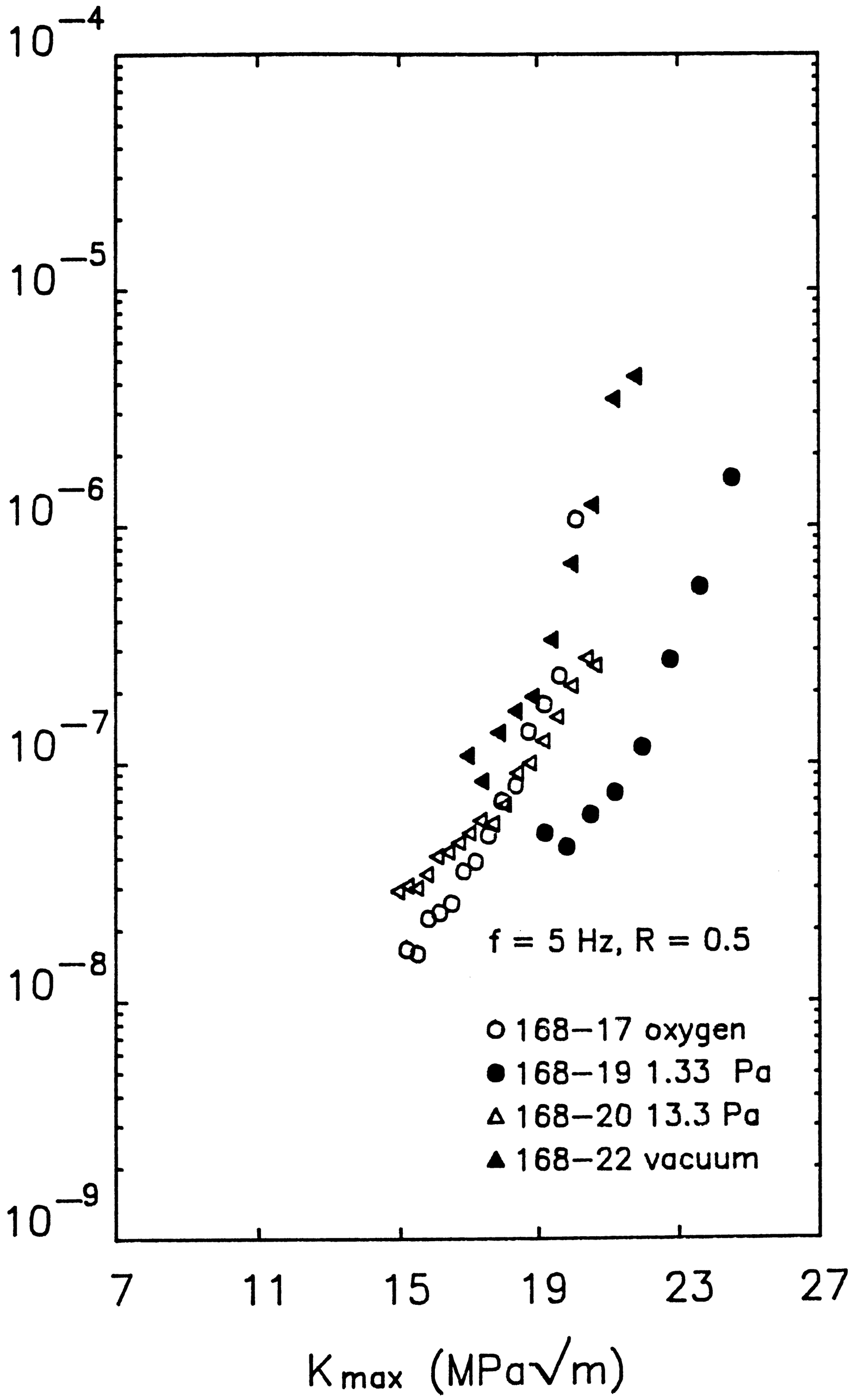


Figure 13: Comparison of fatigue crack growth rate versus $K_{max}$ data for specimens 17, 19, 20, and 22 tested at a load ratio of R = 0.5 in different environments.

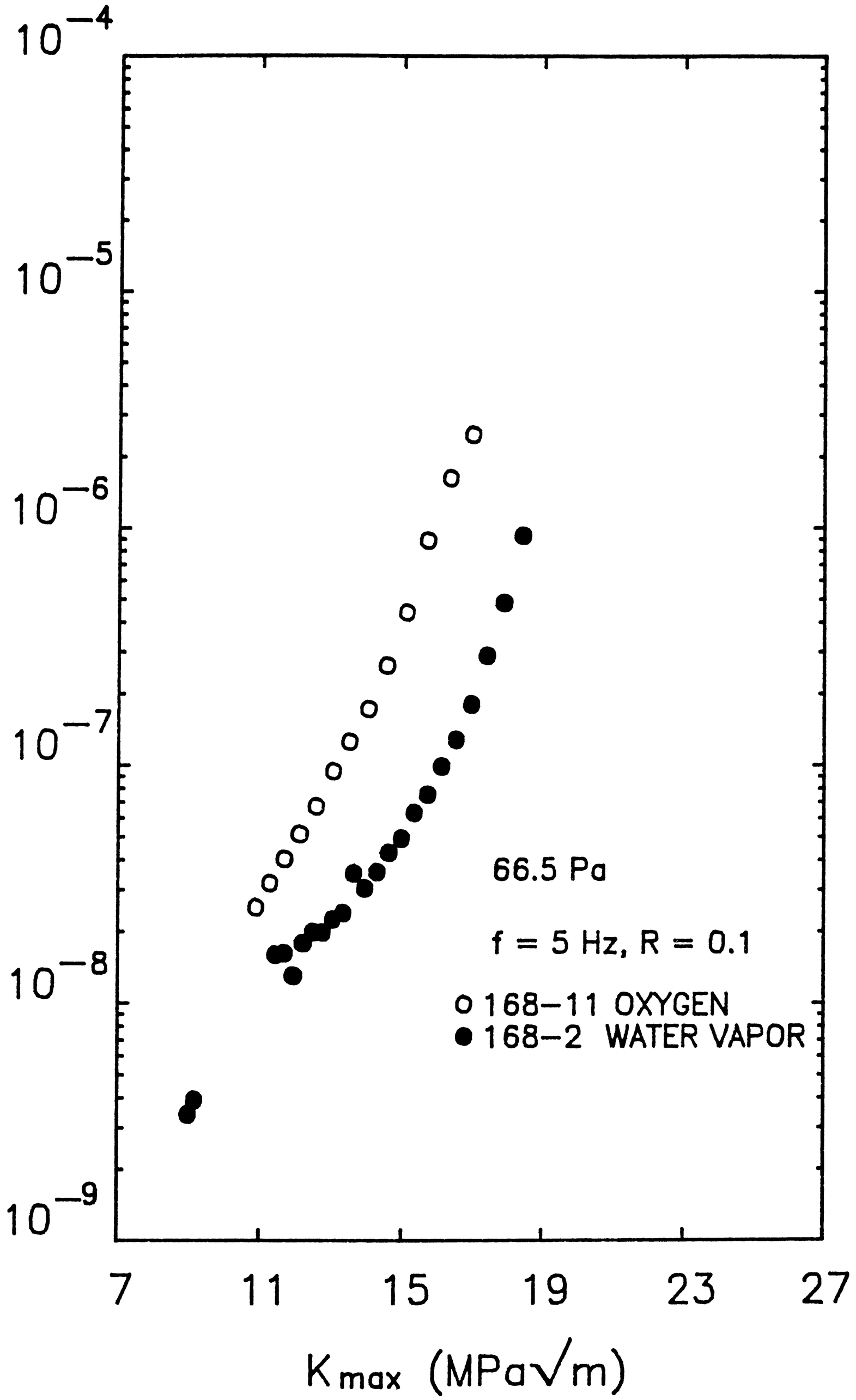


Figure 14: Fatigue crack growth rate versus $K_{max}$ data for specimens 2 and 11 tested in water vapor at 66.5 Pa and in oxygen at 66.5 Pa, respectively.

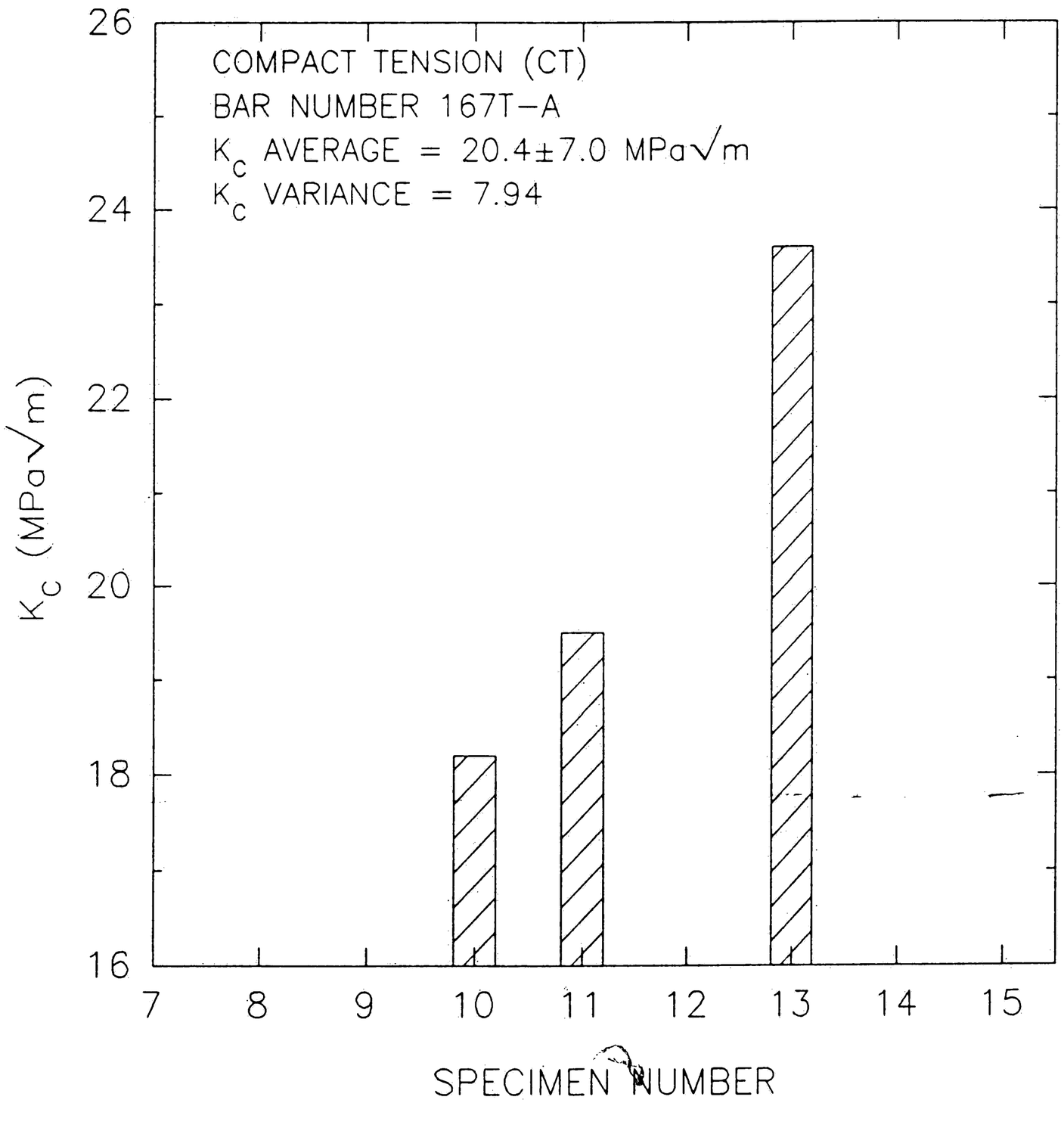


Figure 15: Fracture toughness for compact tension (CT) specimens tested within bar number 167T-A.

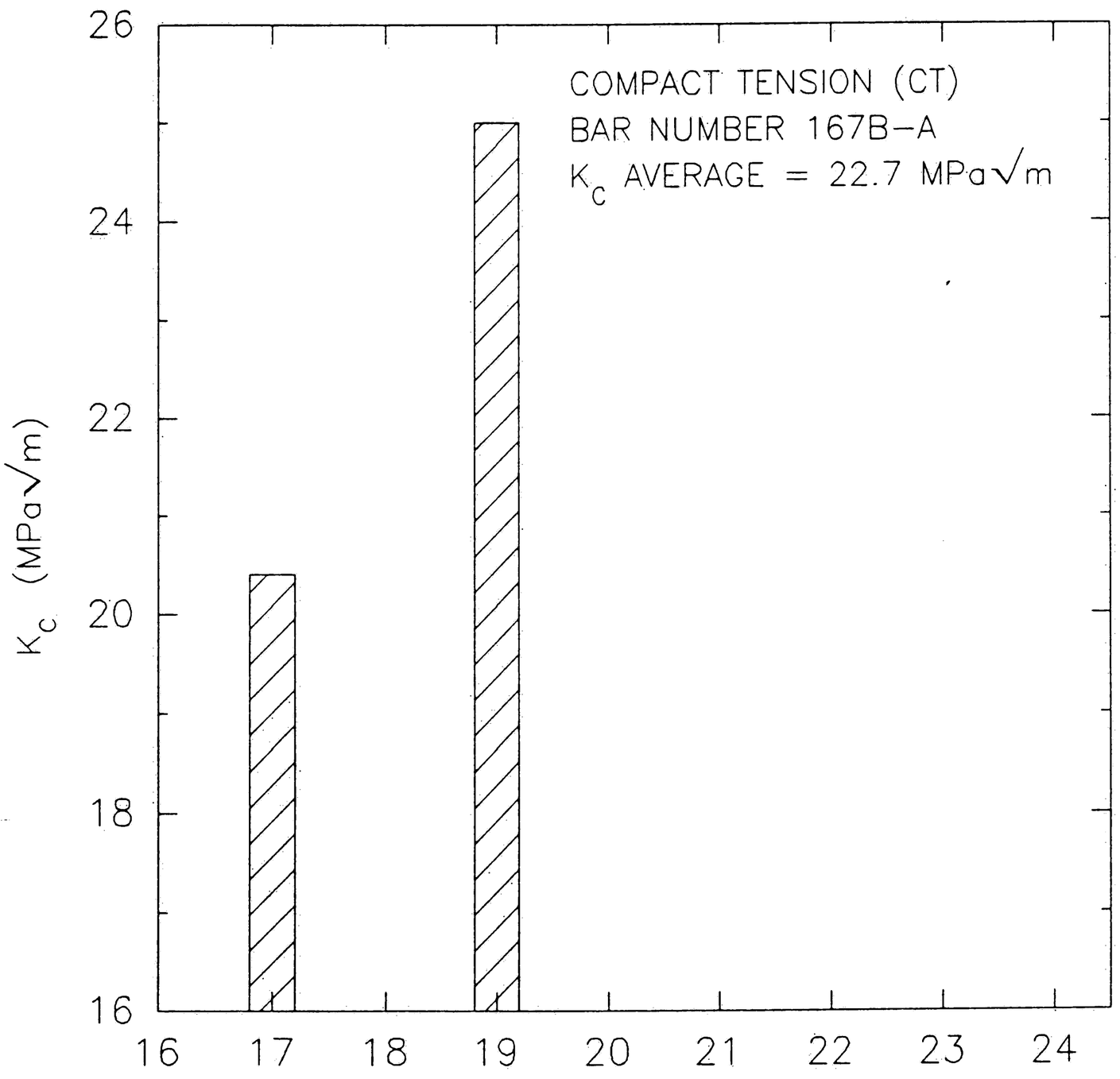


Figure 16: Fracture toughness for compact tension (CT) specimens tested within bar number 167B-A.

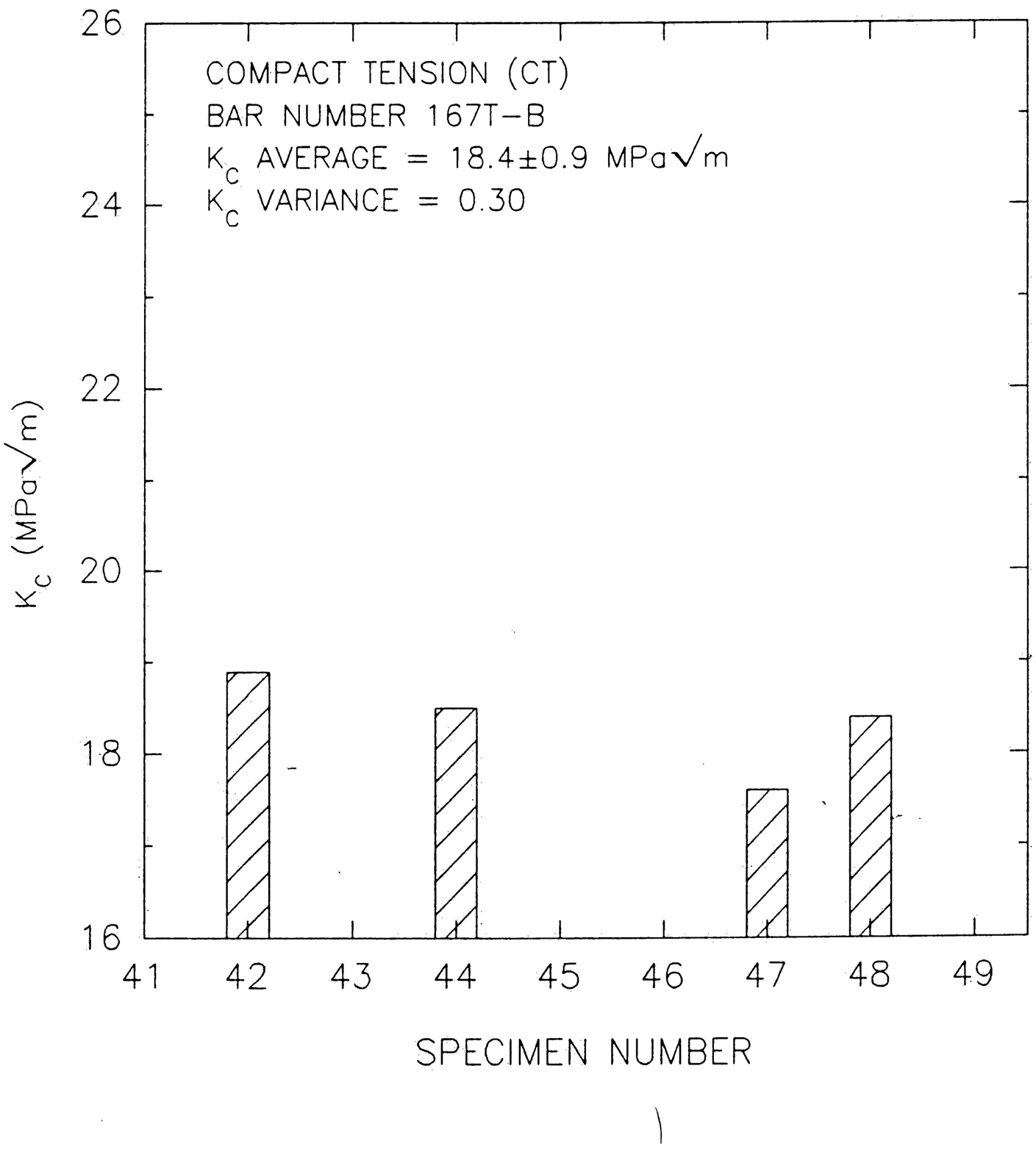


Figure 17: Fracture toughness for compact tension (CT) specimens tested within bar number 167T-B.

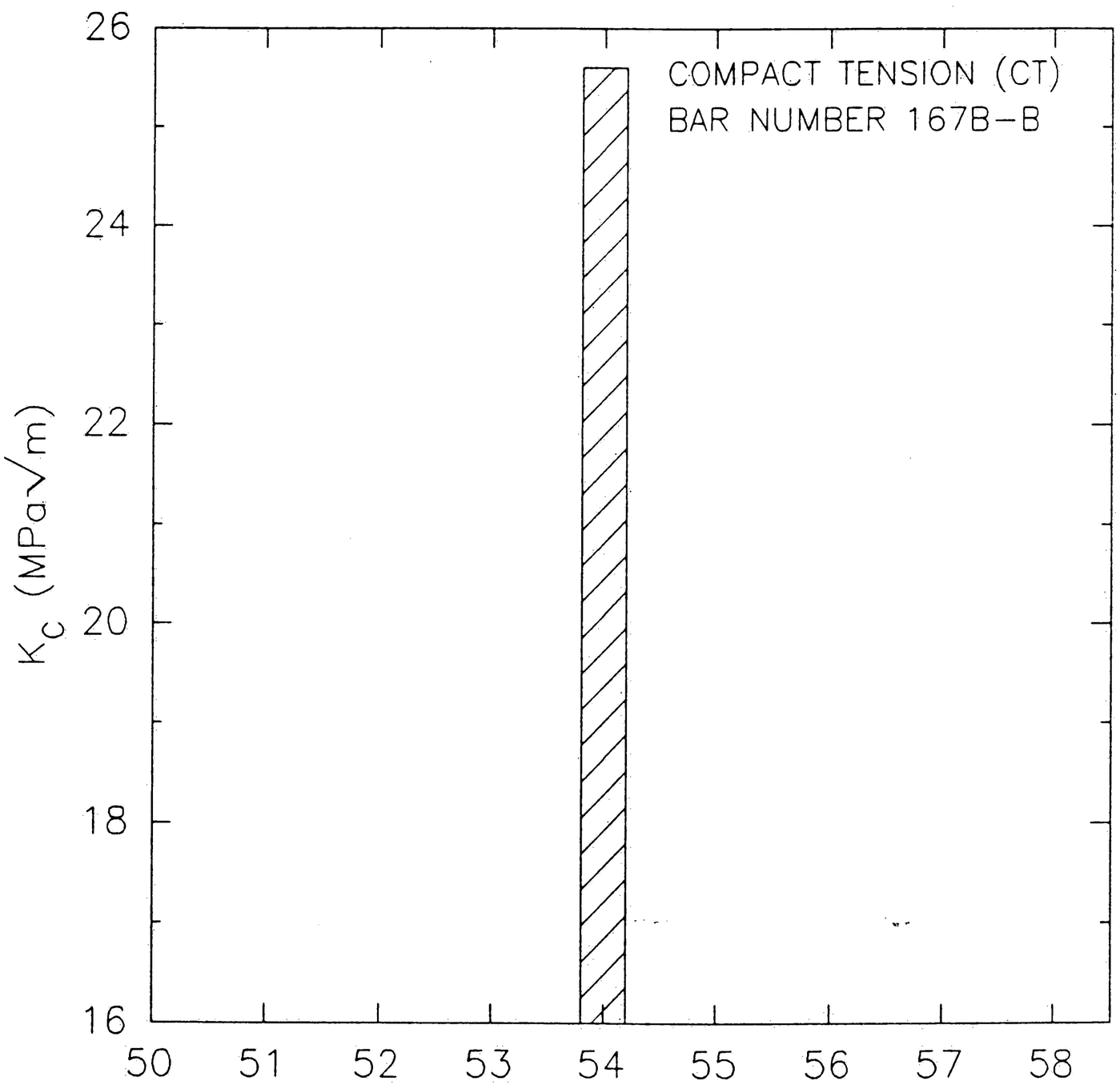


Figure 18: Fracture toughness for compact tension (CT) specimens tested within bar number 167B-B.

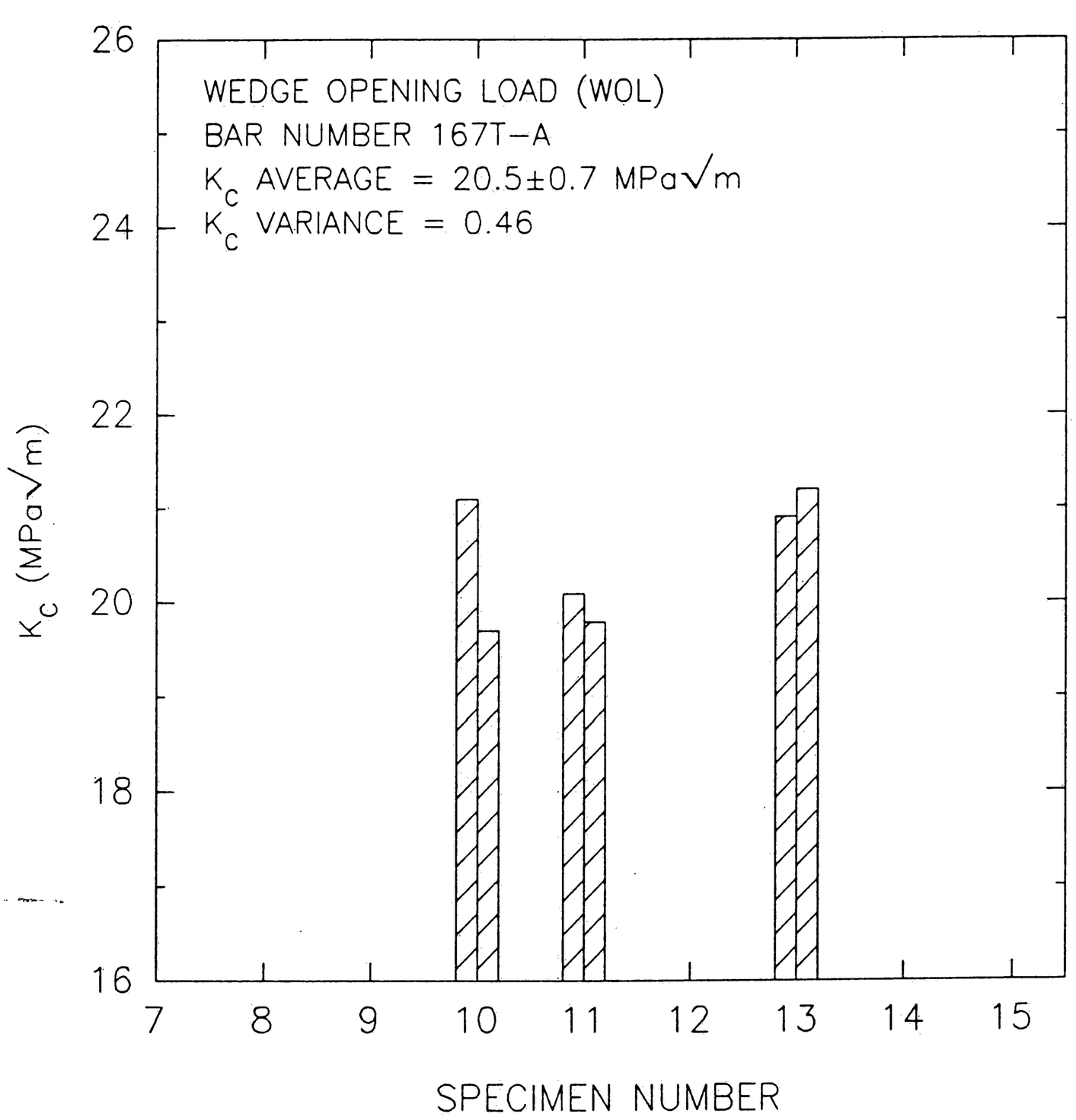


Figure 19: Fracture toughness for wedge opening load (WOL) specimens tested within bar number 167T-A.

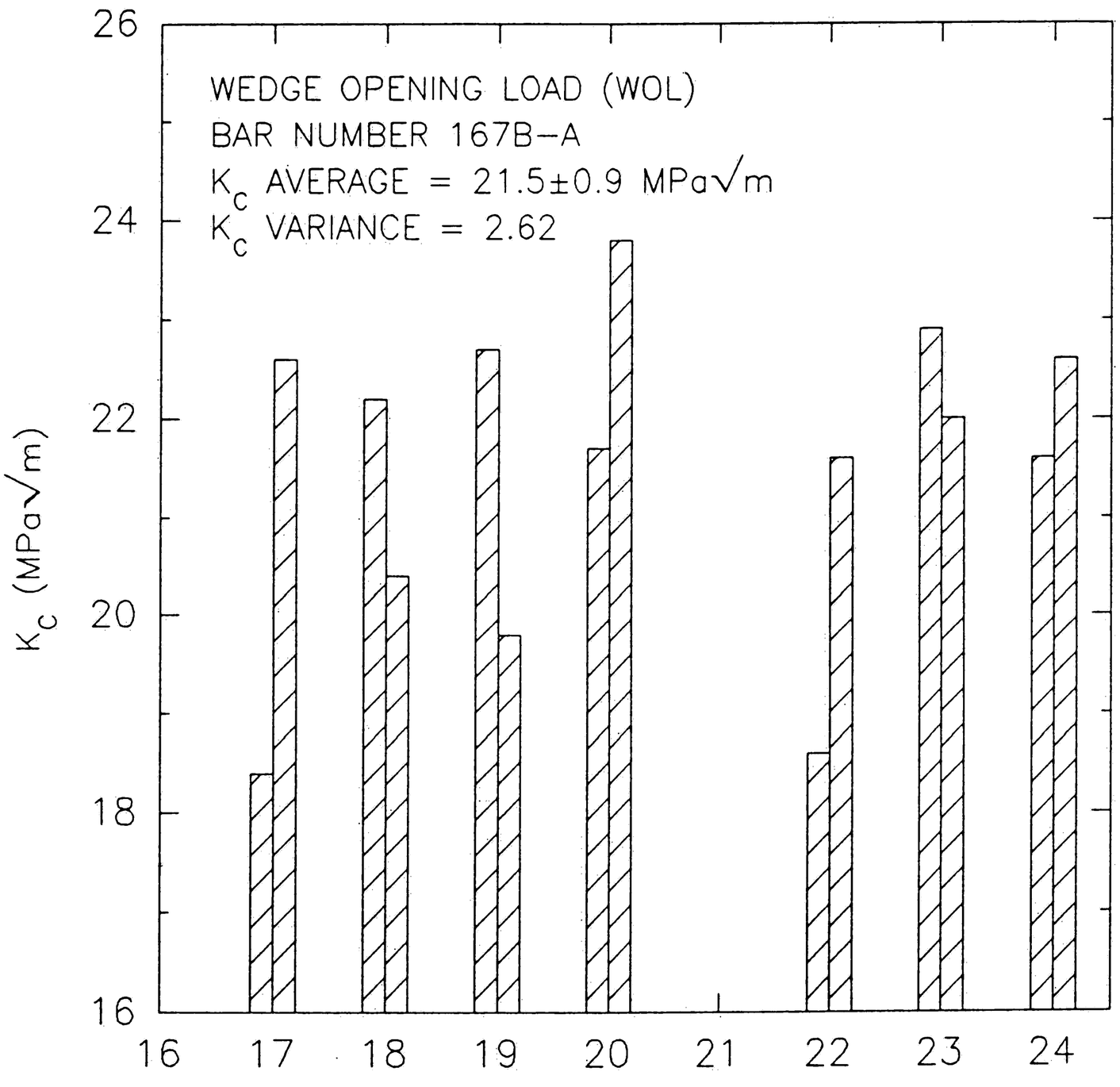


Figure 20: Fracture toughness for wedge opening load (WOL) specimens tested within bar number 167B-A.

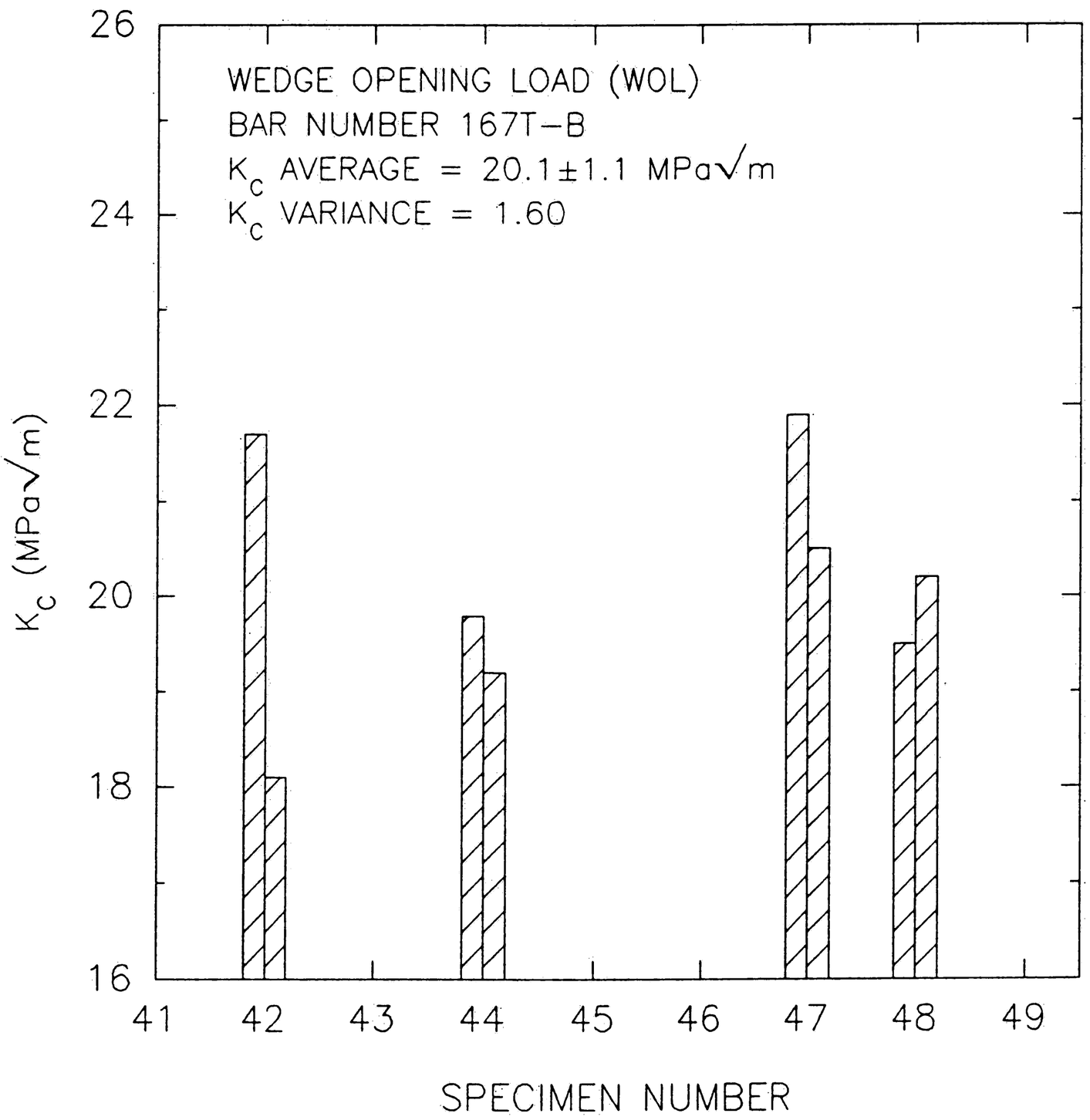


Figure 21: Fracture toughness for wedge opening load (WOL) specimens tested within bar number 167T-B.

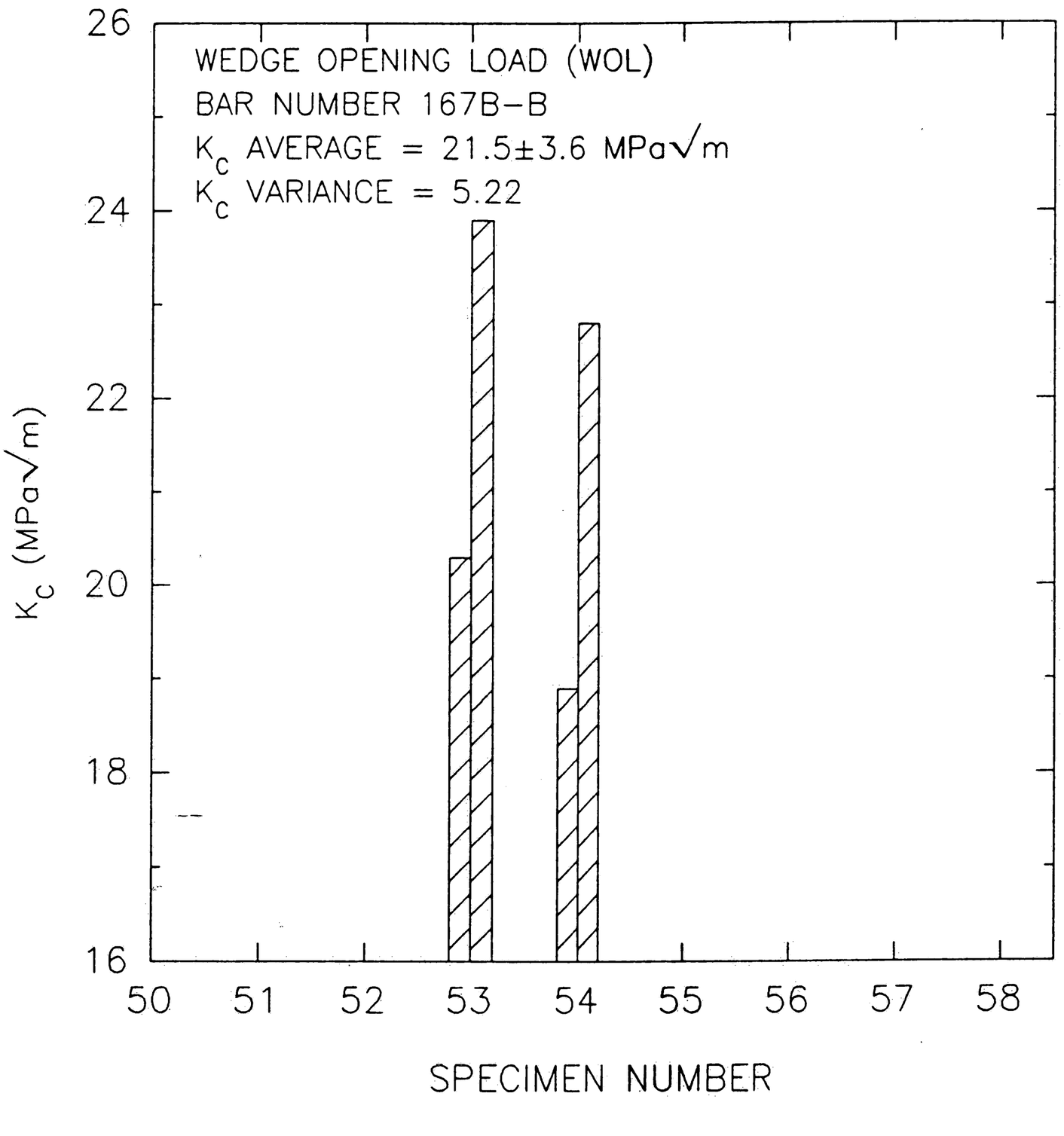


Figure 22: Fracture toughness for wedge opening load (WOL) specimens tested within bar number 167B-B.

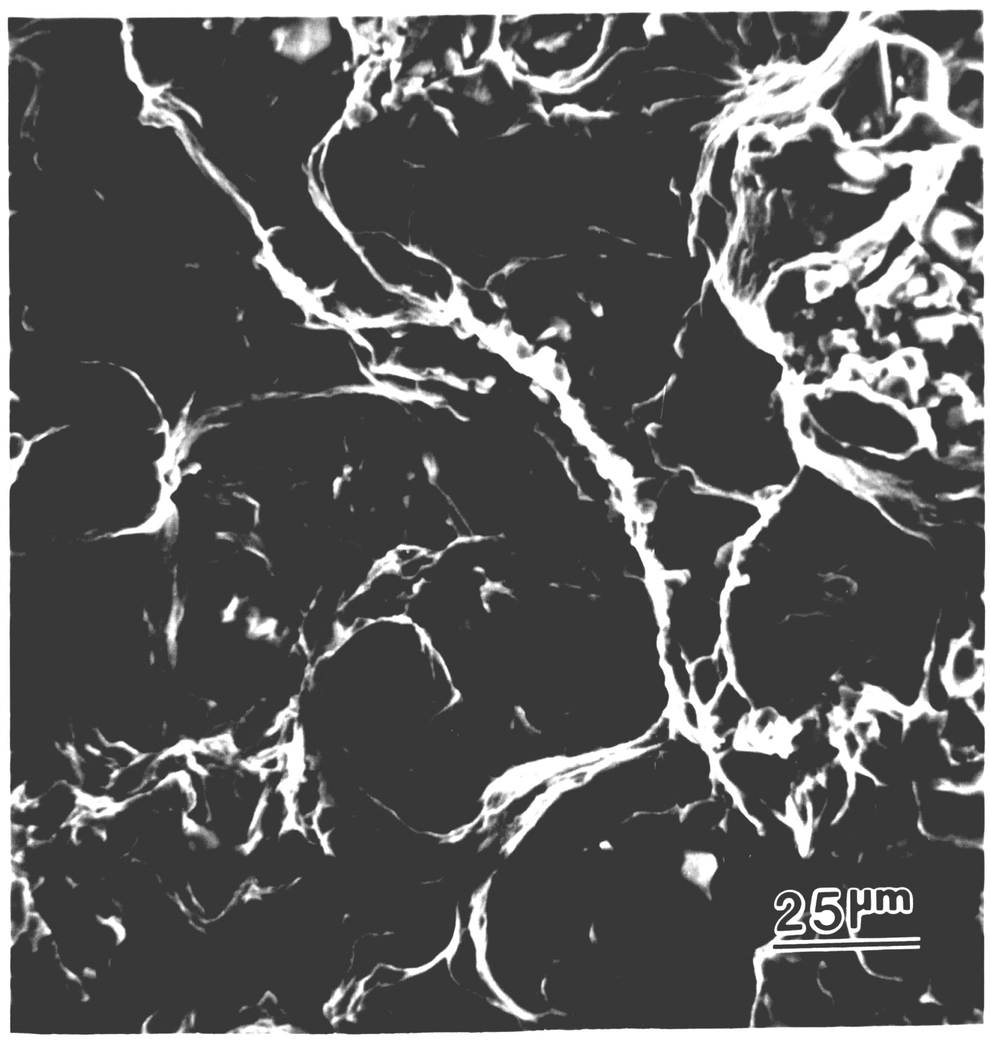





Figure 23: SEM microfractographs of the compact tension (CT) specimen 23 tested in vacuum. $K_{max}$ = 15 MPa-$m^{1/2}$, da/dN = 3.6E-7 m/cycle Magnification: 500X. 15°tilt

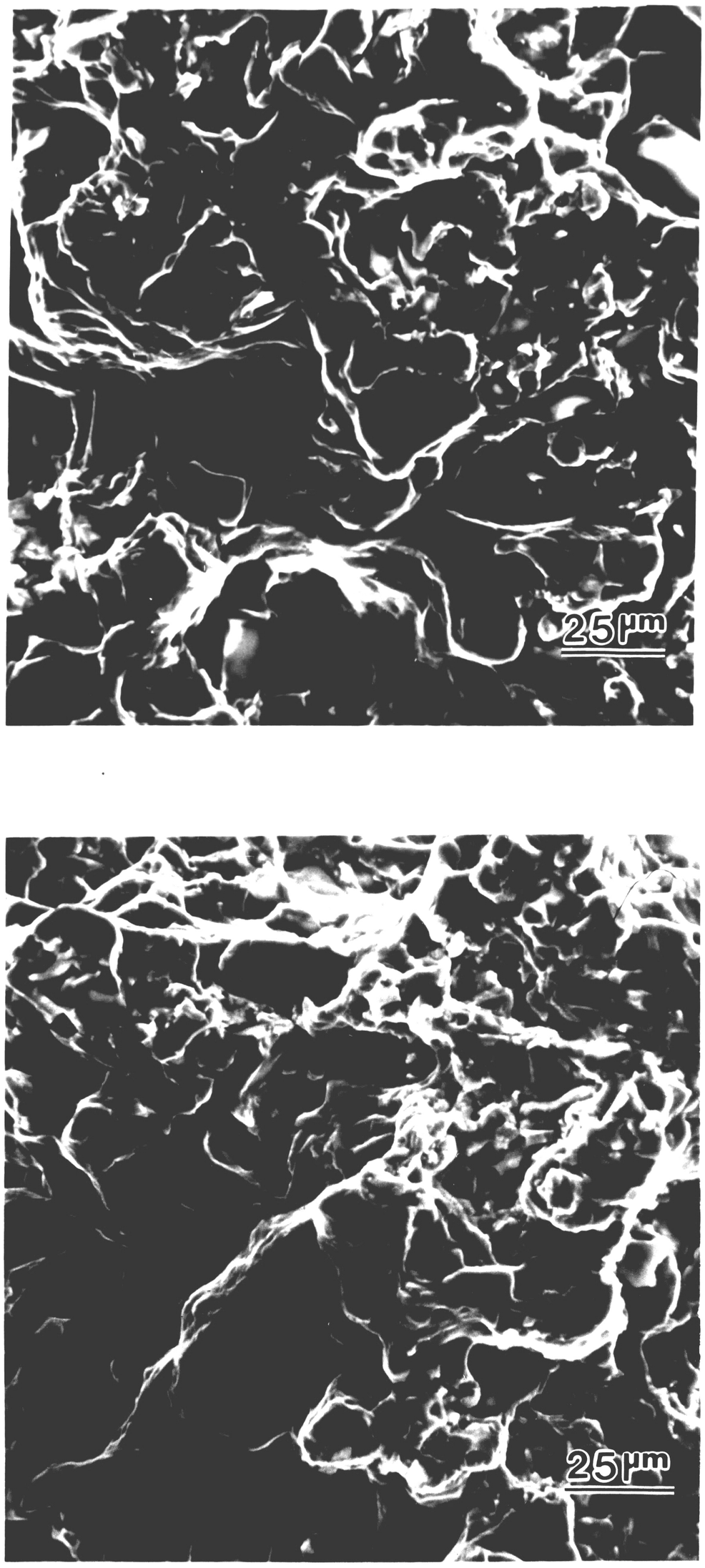


Figure 24: SEM microfractographs of the compact tension (CT) specimen 23 tested in vacuum. $K_{max}$ = 15 MPa-$m^{1/2}$, da/dN = 3.6E-7 m/cycle Magnification: 500X. 15°tilt

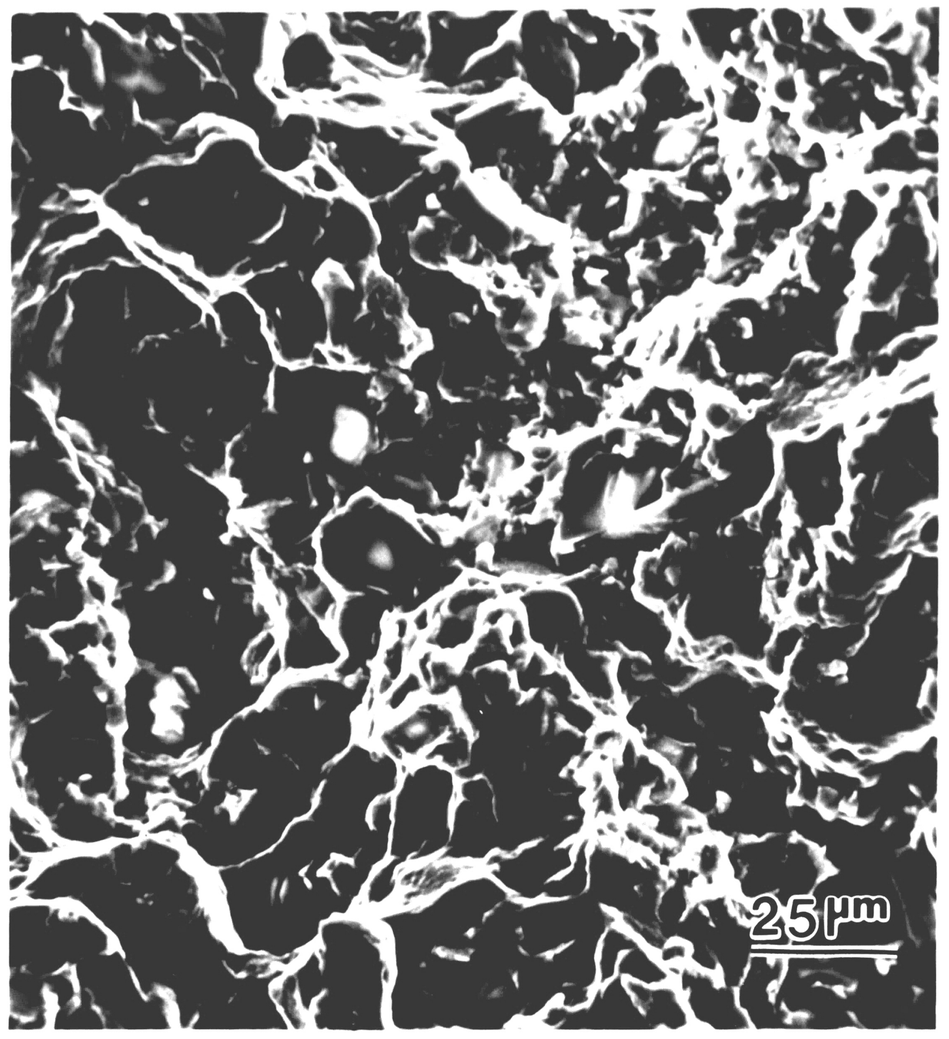



Figure 25: SEM microfractographs of the compact tension (CT) specimen 44 tested in vacuum. $K_{max}$ = 15 MPa-$m^{1/2}$, da/dN = 1.5E-6 m/cycle Magnification: 500X. 15°tilt

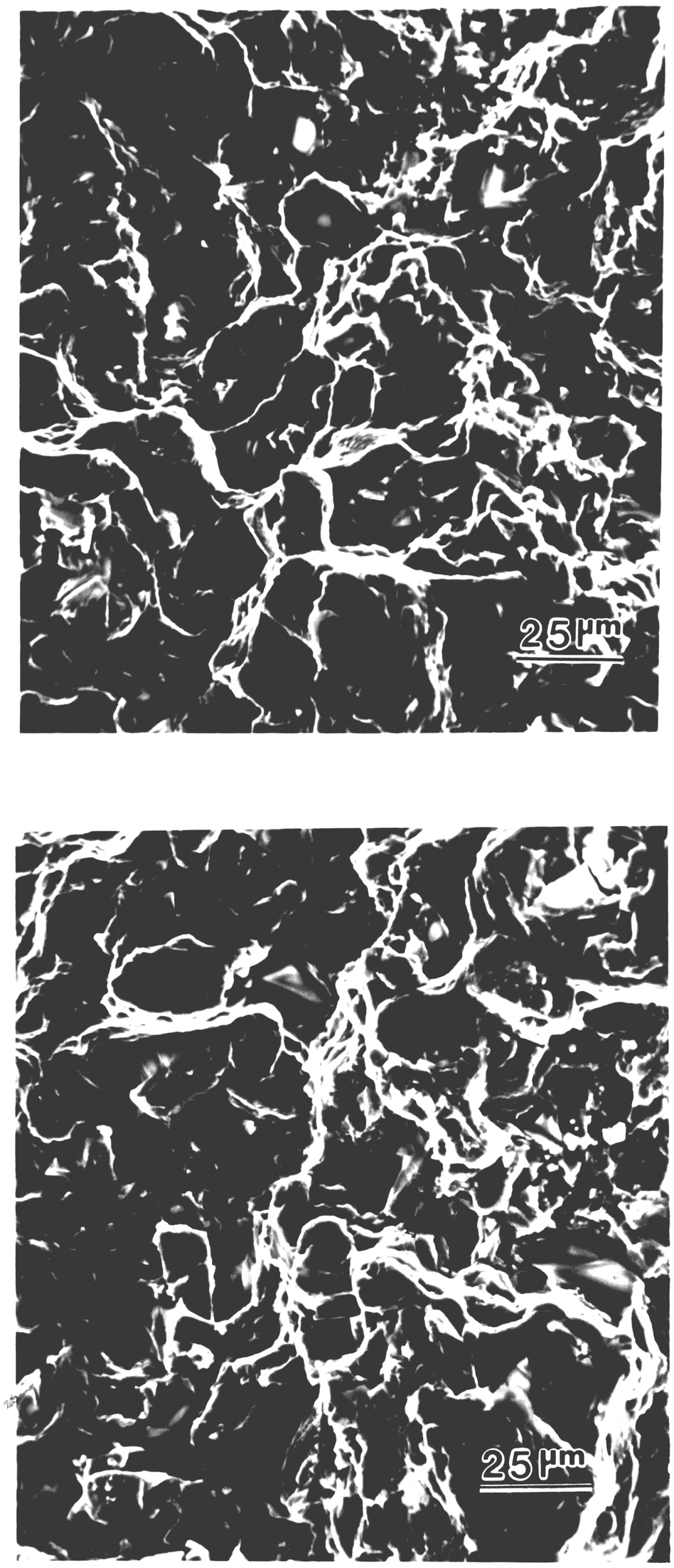


Figure 26: SEM microfractographs of the compact tension (CT) specimen 44 tested in vacuum. $K_{max}$ = 15 MPa-$m^{1/2}$, da/dN = 1.5E-6 m/cycle Magnification: 500X. 15°tilt

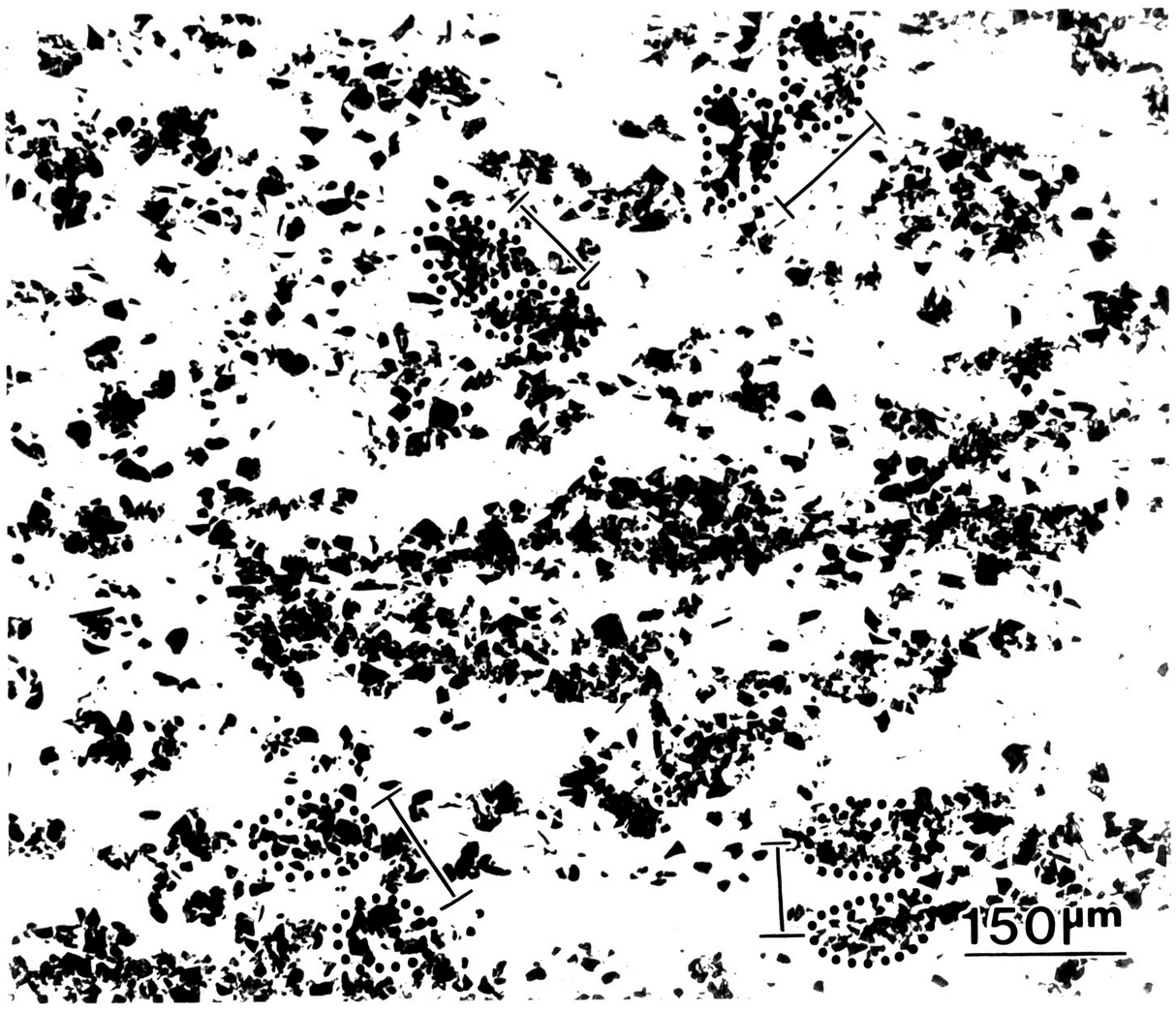


Figure 27: Optical micrograph of specimen 24 showing regions with clusters of alumina particles

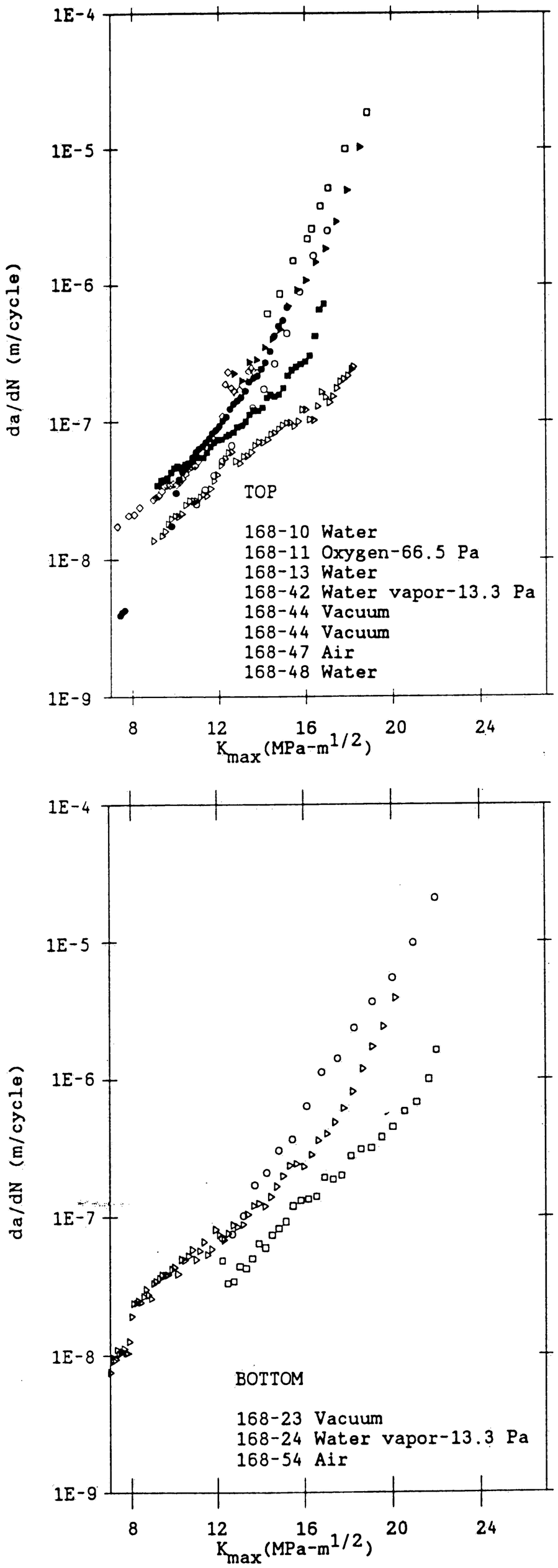


Figure 28: Composite fatigue crack growth rates for the top and bottom of the cast ingots. f = 5Hz, R = 0.1

## REFERENCES


1. Metals Handbook Ninth Edition, "Introduction to Aluminum and Aluminum alloys," 1979, Vol.2, pp. 3-23.

2. Evans, D. G., Morris, P. L., Hains, R. W., Jowett, C., and Achim, P., "Production Extrusion of AA6061-SiC Metal Matrix Composites," Dural Aluminum Composites Corporation, 1988.

3. Dural Aluminum Composites Corporation, "Tomorrow's Metal Matrix Composite, Available and Affordable Today," 1988.

4. Flinn, R. A., and Trojan, P. K., Engineering Materials and their Applications, 2nd Edition. Boston: Houghton Mifflin Co., 1981, p. 434.

5. Dural Aluminum Composites Corporation, "The Dural MMC Process," 1988.

6. Lloyd, D. J., "The Solidification Microstructure of Particulate Reinforced Aluminum/SiC Composites," Composites Science and Technology, 35, 1989, pp. 159-179.

7. Lloyd, D. J., Lagace, H., McLeod, A., and Morris, P. L., "Microstructural Aspects of Aluminum-Silicon Carbide Particulate Composites Produced by a Casting Method," Materials Science and Engineering, A107, 1989, pp. 73-80.

8. Lloyd, D. J., and Dewing, E., "Stability in Molten Aluminum," Proc. International Symposium on Advanced Structural Materials, Ed. D. S. Wilkinson, Pergammon Press, 1988, pp. 71-77.

9. Lloyd, D. J., "Metal Matrix Composites - An Overview," Proc. International Symposium on Advanced Structural Materials, Ed. D. S. Wilkinson, Pergammon Press, 1988.

10. Davidson, D. L., "The Growth of Fatigue Cracks Through Particulate SiC Reinforced Aluminum Alloys," Proceedings of the 7th International Conference on Fracture (ICF7), 1989, pp. 3021-3028.

11. Masuda, C., and Tanaka, Y., "Tensile and Fatigue Properties of SiC Whiskers and SiC Particulate Reinforced Aluminum Composites," Proceedings of the 7th International Conference on Fracture (ICF7), 1989, pp. 3089-3095.

12. You, C. P., and Allison, J. E., "Fatigue Crack Growth and Closure in a $SiC_p$ - Reinforced Aluminum Composite," Proceedings of the 7th International Conference on Fracture (ICF7), 1989, pp. 3005-3011.

13. Logsdon, W. A., and Liaw, P. K., "Tensile, Fracture Toughness and Fatigue Crack Growth Rate Properties of Silicon Carbide Whisker and Particulate Reinforced Aluminum Metal Matrix Composites," Engineering Fracture Mechanics, Vol.24, No.5, 1986, pp. 737-751.

14. Shang, J. K., and Ritchie, R. O., "On the Particle-Size Dependance of Fatigue Crack Propagation Thresholds SiC-Particulate-Reinforced Aluminum-Alloy Composites: Role of Crack Closure and Crack Trapping," Acta. Metall., Vol.37, No.8, 1989, pp. 2267-2278.

15. Lewandowski, J. J., and Liu, C., "Effects of Matrix Microstructure and Particle Distribution on Fracture of an Aluminum Metal Matrix Composite," Materials Science and Engineering, A107, 1989, pp. 241-255.

16. Kamat, S. V., Hirth, J. P., and Mehrabian, R., "Mechanical Properties of Particulate-Reinforced Aluminum-Matrix Composites," Acta Metall., Vol.37, No.9, 1989, pp. 2395-2402.

17. Flom, Y., and Arsenault, R. J., "Effect of Particle Size on Fracture Toughness of SiC/Al Composite Material," Acta Metall., Vol.37, No.9, 1989, pp. 2413-2423.

18. Manoharan, M., Liu, C., and Lewandowski, J. J., "Microstructure and Particle Size Effects on Fracture in Aluminum Metal Matrix Composites," Proceedings of the 7th International Conference on Fracture (ICF7), 1989, pp. 2977-2985.

19. Private conversation with Wei, R. P., Lehigh University, 1989.

20. Klimowicz, T. F., and Vecchio, K. S., "The Influence of Aging Condition on the Fracture Toughness of Alumina-Reinforced Aluminum Composites," Report Presented at TMS Fall, Indianapolis, 1989.

21. Metals Handbook Ninth Edition, "Environmental Effects on Fatigue Crack Propagation," 1979, Vol.8, pp. 403-410.

22. Gao, Ming, Unpublished Results, Lehigh University, 1989.

23. Chin, Gary, Unpublished Results, Lehigh University, 1989.

24. "Standard Test Method for Measurement of Fatigue Crack Growth Rates," E647, Annual Book of ASTM Standards, Vol.03.01, 1988, pp. 636-654.

25. "Standard Test Method for Plane-Strain Fracture Toughness of Metallic Materials," E399, Annual Book of ASTM Standards, Vol.03.01, 1983, pp. 480-504.

26. Saxena, A., Hudak, S. J., Donald, J. K., and Schmidt, J., Testing Evaluation, 167, 1978.

27. User's Reference Manual for Automated Fatigue Crack Growth, Version 2.40, 1988.

28. Saxena, A., and Hudak, S. J., "Review and Extension of Compliance Information for Common Crack Growth Specimens," Int. J. Fracture, Vol.14, 1978, pp. 453-468.

29. Wei, R. P., and Brazil, R. L., "An Assessment of A-C and D-C Potential Systems for Monitoring Fatigue Crack Growth," Fatigue Crack Growth Measurement and Data Analysis, ASTM STP738, S. J. Hudak, Jr., and R. J. Bucci, Eds., American Society for Testing and Materials, 1981, pp. 103-119.

30. Hahn, G. T., and Rosenfield, A. R., "Metallurgical Factors Affecting Fracture Toughness of Aluminum Alloys," Metall. Trans A 6A, 1975, pp.653-668.

31. Rice, J. R., and Johnson, M. A., Inelastic Behavior of Solids, M. F. Kanninen, ed., McGraw-Hill, 1970, p. 641.

32. Krafft, G. T., "Correlation of Plane Strain Crack Toughness with Strain Hardening Characteristics of a Low, a Medium, and a High Strength Steel," Appl. Mater. Res., 1, 1964, pp. 88-101.

33. Aerospace Structural Metals Handbook, Belfour Stulen, Inc., 1971.

# APPENDIX I

## DATA FOR THE COMPACT TENSION (CT)

## SPECIMEN TESTING

| Specimen | $P_{pop\text{-}in}$ ($10^2$ N) | $P_{max}$ ($10^2$ N) | $a_{measured}$ (mm) | $a_{corrected}$ (mm) | Kc (MPa-$m^{1/2}$) |
|---|---|---|---|---|---|
| 02 | ----- | 42.26 | 30.07 | ----- | 21.9 |
| 10 | 41.63 | 42.08 | 27.20 | 27.57 | 18.2 |
| 11 | ----- | 67.38 | 20.68 | ----- | 19.5 |
| 13 | 52.84 | 31.09 | 27.28 | 27.60 | 23.6 |
| 17 | ----- | 53.80 | 25.44 | ----- | 20.4 |
| 19 | ----- | 54.05 | 28.52 | ----- | 25.0 |
| 42 | ----- | 56.38 | 23.34 | ----- | 18.9 |
| 44 | ----- | 49.09 | 25.30 | ----- | 18.5 |
| 47 | 40.65 | 40.65 | 27.48 | ----- | 17.5 |
| 48 | 40.79 | 40.79 | 28.17 | ----- | 18.4 |
| 54 | ----- | 44.48 | 31.44 | ----- | 25.6 |

# APPENDIX II

# DATA FOR THE WEDGE OPENING LOAD (WOL)

# SPECIMEN TESTING

| Specimen | $P_{pop\text{-}in}$ ($10^2$ N) | $P_{max}$ ($10^2$ N) | $a_{measured}$ (mm) | $a_{corrected}$ (mm) | Kc (MPa-$m^{1/2}$) |
|---|---|---|---|---|---|
| 02-A | ----- | 13.83 | 14.13 | ----- | 17.5 |
| 02-B | 18.19 | 19.13 | 11.74 | 11.85 | 19.1 |
| 10-A | 18.90 | 20.37 | 11.91 | 12.25 | 21.1 |
| 10-B | 17.61 | 18.95 | 11.82 | 12.29 | 19.7 |
| 11-A | 17.92 | 18.90 | 12.02 | 12.48 | 20.1 |
| 11-B | 18.37 | 19.26 | 11.92 | 12.15 | 19.8 |
| 13-A | 18.90 | 19.88 | 11.83 | 12.40 | 20.9 |
| 13-B | 19.44 | 20.99 | 11.45 | 11.98 | 21.2 |
| 17-A | ----- | 13.83 | 14.50 | ----- | 18.4 |
| 17-B | 19.44 | 21.22 | 11.60 | 12.50 | 22.6 |
| 18-A | 17.93 | 19.84 | 12.30 | 13.00 | 22.2 |
| 18-B | 17.61 | 18.73 | 12.35 | 12.74 | 20.4 |
| 19-A | 19.97 | 21.75 | 11.64 | 12.29 | 22.7 |
| 19-B | 17.57 | 18.55 | 12.37 | 12.55 | 19.8 |
| 20-A | 19.04 | 20.82 | 11.70 | 12.29 | 21.7 |
| 20-B | 22.46 | 24.24 | 11.30 | 11.65 | 23.8 |
| 22-A | 15.70 | 16.64 | 12.88 | 12.98 | 18.6 |
| 22-B | 20.10 | 21.39 | 11.80 | 11.94 | 21.6 |
| 23-A | 18.82 | 20.28 | 11.93 | 13.08 | 22.9 |
| 23-B | 19.26 | 20.37 | 12.00 | 12.67 | 22.0 |
| 24-A | 19.48 | 21.57 | 11.63 | 11.88 | 21.6 |
| 24-B | 20.42 | 21.75 | 11.63 | 12.24 | 22.6 |

| Specimen | $P_{pop\text{-}in}$ ($10^2$ N) | $P_{max}$ ($10^2$ N) | $a_{measured}$ (mm) | $a_{corrected}$ (mm) | $K_c$ (MPa-$m^{1/2}$) |
|---|---|---|---|---|---|
| 42-A | 20.28 | 21.35 | 11.80 | 12.04 | 21.7 |
| 42-B | 17.97 | 17.97 | 11.92 | ----- | 18.1 |
| 44-A | 18.73 | 19.88 | 11.58 | 11.82 | 19.8 |
| 44-B | 17.61 | 18.73 | 11.85 | 12.11 | 19.2 |
| 47-A | 18.82 | 20.51 | 11.92 | 12.43 | 21.9 |
| 47-B | 18.10 | 19.70 | 11.79 | 12.29 | 20.5 |
| 48-A | 18.55 | 19.39 | 11.67 | 11.90 | 19.5 |
| 48-B | 19.26 | 20.91 | 11.69 | 12.03 | 20.2 |
| 53-A | 19.17 | 20.24 | 11.72 | 11.87 | 20.3 |
| 53-B | 22.55 | 23.62 | 11.52 | 11.99 | 23.9 |
| 54-A | 18.68 | 18.68 | 11.99 | 12.00 | 18.9 |
| 54-B | 21.35 | 22.82 | 11.39 | 11.84 | 22.8 |

# VITA

Eda Emine Topur was born in Washington D.C. on July 28, 1967 to Tuncer and Cigdem Topur of Istanbul, Turkey. She attended Dickinson College in Carlisle, PA for two years starting in August, 1984. Transferring to Lehigh University in Bethlehem, PA , she received a Bachelor's Degree in Mechanical Engineering in January, 1989.

Following receipt of her B.S., she began a Master's Degree program in Applied Mechanics, working under Dr. Robert P. Wei at Lehigh University in January, 1989.